University of Alberta

Periodic Solutions and Bistability in a Model for Cytotoxic T-Lymphocyte (CTL) Response to Human T-Cell Lymphotropic Virus Type 1 (HTLV-I)

by

John Cameron Lang

A thesis submitted to the Faculty of Graduate Studies and Research
in partial fulfillment of the requirements for the degree of

Master of Science
in
Applied Mathematics

Department of Mathematics and Statistical Sciences

Fall 2009
Edmonton, Alberta

Examining Committee

Michael Y. Li, Mathematics and Statistical Sciences

James S. Muldowney, Mathematics and Statistical Sciences

Jack A. Tuszynski, Physics

To my parents, brother, and fiancée.

Abstract

HTLV-I is the first discovered human retrovirus and a causative agent of both adult T-cell leukemia (ATL) and HTLV-I-associated myelopathy (or tropical spastic paraparesis) (HAM/TSP). Previous models have been successful in providing insight into the progression of HTLV-I infection. The relative simplicity of HTLV as well as its similarities to HIV and other diseases allow HTLV-I research to have diverse applications.

The development of HAM/TSP is precipitated by a CTL immune response. Previous models for CTL response to HTLV-I infection have had relatively simple behaviours. A novel sigmoidal CTL response function results in complex behaviours previously unobserved. We establish the existence of bistability between solutions corresponding to carrier and endemic states. In addition, both super- and sub-critical Hopf bifurcations as well as the resulting stable and unstable periodic solutions are observed. Analytical and numerical results are discussed, as well as the biological consequences of the aforementioned behaviours.

I am deeply grateful for the excellent support and guidance of my supervisor.

I would also like to acknowledge the financial support of the National Sciences and Engineering Research Council of Canada, the University of Alberta and the Department of Mathematics and Statistical Sciences, and the Government of Alberta.

Contents

List of Tables

List of Figures

Chapter 1

Introduction

1.1 Background

Human T-cell leukemia/lymphoma virus type I (HTLV-I) is the first discovered human retrovirus [8]. Shortly after its discovery HTLV-I was linked as a causative agent of adult T-cell leukemia (ATL) [8, 21] as well as HTLV-I-associated myelopathy (or tropical spastic paraparesis) (HAM/TSP) [13, 27]. HTLV-I is endemic to regions of Japan, Latin America, and Africa and has been estimated to infect between 10 and 20 million individuals worldwide as of 1993 [6, 7].

The mechanism by which HTLV-I infection causes either ATL or HAM/TSP is not entirely understood. Due to the problematic nature of investigating in-host disease dynamics experimentally mathematical models are important tools for exploring HTLV-I infection. Fortunately, the relatively simple nature of the HTLV-I virus makes it an excellent candidate for mathematical modelling. Models constructed to explain both the development of ATL [10, 31] and HAM/TSP [9, 11, 32, 33] have contributed significant insights into the progression of HTLV-I infection.

The common features HTLV-I shares with other diseases allows us to contribute insight to many other areas. For example, studying HTLV-I can help lay a firm

foundation for the modelling of the closely related, but more complicated, HIV virus. In this instance the modelling is simplified by the low mutation rate of HTLV-I [16] and the lack of free HTLV-I particles in vivo [4]. In a more abstract fashion, techniques developed to model ATL can be applied to study other oncoviruses. Similarly, insights into HAM/TSP may be useful to the study of other autoimmune disorders, regardless of whether or not they are triggered by viral infection.

1.2 HTLV-I

We now summarize various reviews of HTLV-I [1, 4, 19].

The primary target of HTLV-I are $CD4^+$ T-cells. Indeed, HTLV-I virions do not exist as cell-free viral particles and are confined to $CD4^+$ T-cells. A $CD4^+$ T-cell which has been infected by the HTLV-I virus is referred to as a proviral cell. This leads to two different modes of viral replication. First, direct contact between a proviral cell and a healthy $CD4^+$ T-cell may result in a transmission of HTLV-I. Second, since HTLV-I is a retrovirus, mitosis of a proviral cell produces two new proviral cells. In the case of direct contact it is clear that HTLV-I genes must be active in order for there to be virions present to transfer between cells. In the second case it is possible for mitosis to occur either as a result of HTLV-I expression or as a result of the normal cell cycle. The latter feature is very interesting as it provides a mechanism for HTLV-I replication which is undetectable by the human immune response.

In response to HTLV-I infection the human immune system mounts a strong and sustained cytotoxic T-lymphocyte (CTL) response. These killer T-cells are able to identify and destroy proviral cells expressing the HTLV-I genome. Most CTLs target the HTLV-I protein Tax. Again, it is important to note that the CTL response is ineffective against proviral cells not expressing the HTLV-I genome.

HTLV-I cannot be eliminated by the human immune system, and hence, persists for life. Even so, less than 5% of those infected with HTLV-I develop either ATL or HAM/TSP . Moreover, these diseases are developed only after a very long incubation period of between 20 and 30 years . Why this is the case is not fully understood and gives rise to two fundamental, yet unresolved, questions:

1. Why is it that some people infected with HTLV-I remain asymptomatic carriers and only a few develop either ATL or HAM/TSP?, and
2. Why is it that disease develops after such a long incubation period?

These questions are subjects of extensive immunological studies. Mathematical modelling has and continues to be used as a tool to provide insight into these outstanding problems [9, 10, 11, 31, 32, 33]. Below we focus our efforts on these two questions as they pertain to HTLV-I-associated HAM/TSP.

1.3 Proposed Pathogenesis

HTLV-I-associated HAM/TSP is a degenerative neurologic disease resulting from demyelination of neurons in the central nervous system (CNS). There are two main hypotheses for the mechanism which results in damage to the CNS. Both hypotheses agree that demyelination is the result of the CTL response [12, 14, 15]; where they diverge is in their explanation of why neurons of the CNS are subject to the CTL response. According to these hypotheses, the CNS is subject to the CTL response because either they become infected by the HTLV-I virus [14] or they express antigens which are cross reactive with those of HTLV-I [12].

Although some resident cells of the CNS are susceptible to the HTLV-I virus [20, 22], the main reservoir of HTLV-I in the CNS are $CD4^+$ cells [25]. Indeed, it has been shown that infiltration of the CNS by $CD4^+$ T-cells immediately precedes damage to the CNS [18]. Since this evidence supports the second hypothesis, we

assume that it is correct. Moreover, assuming the second hypothesis simplifies the modelling effort by reducing the number of cells targeted by the HTLV-I virus.

We now proceed with a brief review of previous mathematical models for HTLV-I dynamics to be followed by the introduction of our model.

1.4 Previous Models

There are three main types of cells which are critical to the modelling effort. It is absolutely necessary to keep track of the primary host cells. So, we track the number of healthy (x) and proviral (y) $CD4^+$ T-cells. Since we are focusing on the development of HTLV-I-associated HAM/TSP and since disease likely results from the CTL response, we also track the number of CTLs (z). We again emphasize that since free HTLV-I virions are rare, there is no need to keep track of free HTLV-I particles.

An excellent summary of basic models for in-host viral dynamics with CTL response is given in Nowak and May (2000), Chapter 6 [26]. It should be noted, however, that these models cannot be directly applied to the situation regarding HTLV-I because of the particular method HTLV-I employs to produce new proviral cells. Recall, HTLV-I does not exist as free virus particles (v) and infects new cells through direct cell-to-cell contact or through mitosis. It is nevertheless insightful to examine the transfer diagram for these systems.

(1.4.1)

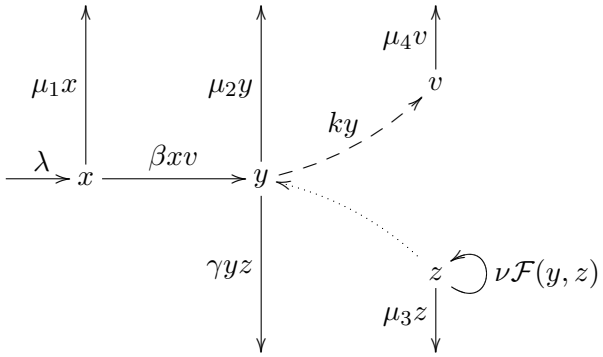

where Nowak and May (2000) [26] explore the functions $\mathcal{F}(y,z) = 1$, $\mathcal{F}(y,z) = y$, and $\mathcal{F}(y,z) = yz$. Which function is most appropriate to model the CTL response is as of yet unknown. Some even suggest that different functions may be appropriate for different individuals [17]. Due to the difficulties in selecting an appropriate response function the primary focus of our model is investigating the effects of a particular family of response functions.

We now make the appropriate modifications to (1.4.1) to reflect the fact that HTLV-I does not exist as free virions and that transmission occurs through cell-to-cell contact. Applying the simplifying assumption to omit the mitosis of healthy and proviral $CD4^+$ T-cells, we then obtain a model proposed by Gomez-Acevedo, Li, and Jacobson (*unpublished*) [9]. This model is summarized in the following transfer diagram and system of differential equations.

(1.4.2)

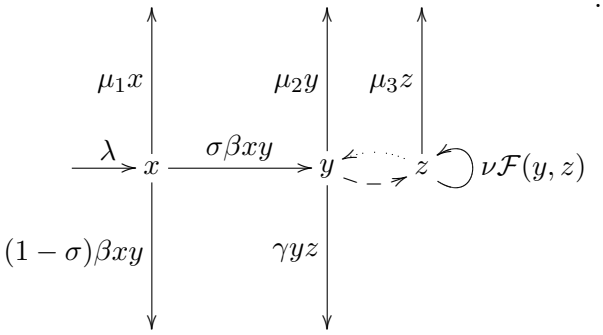

$$\dot{x} = \lambda - \beta xy - \mu_1 x \tag{1.4.3a}$$

$$\dot{y} = \sigma\beta xy - \gamma yz - \mu_2 y \tag{1.4.3b}$$

$$\dot{z} = \nu\mathcal{F}(y,z) - \mu_3 z. \tag{1.4.3c}$$

Gomez-Acevedo, Li, and Jacobson (*unpublished*) [9] use the response function $\mathcal{F}(y,z) = \frac{yz}{z+a}$, where $a \in \mathbb{R}_+$. Since this is the first model introduced that treats HTLV-I specifically, we provide a brief discussion of the model's structure and its results. Following this, we briefly explore two other sophisticated models proposed by Wodarz and Bangham (2000) [32], and Wodarz, Nowak, and Bangham (1999) [33].

1.4.1 Gomez-Acevedo, Li, and Jabobson (*unpublished*) [9]

The primary target of the HTLV-I virus, $CD4^+$ T-cells (x), are assumed to be produced at a constant rate, λ. These healthy cells can only become infected by direct cell-to-cell contact with a proviral $CD4^+$ T-cell (y). The law of mass action allows us to characterize this interaction with the expression βxy. The infectivity, β, represents the ability of a proviral cell to transmit HTVL-I to a susceptible cell. Of course, not every transmission of HTLV-I results in a new proviral cell; for example, the reverse transcription and integration of HTLV-I into the host genome can be fatal. In order to represent this reality it is necessary to introduce the constant $\sigma \in (0,1]$ which represents the probability of a transmission of HTLV-I resulting in a new proviral cell.

Since $CD8^+$ T-cells (z) play a critical role in the immune response to HTLV-I infection and pathogenesis of HAM/TSP, they are also included in the model. The role of these cells is to target and destroy infected $CD4^+$ T-cells. We again apply the law of mass action to characterize this interaction as γyz. The constant γ represents the cytotoxic responsiveness of the system. In other words, γ is the rate

of CTL-initiated lysis. However, since these killer cells are only able to detect and destroy proviral cells which express the HTLV-I genome, γ must also take into account the fact that at any given moment only a small fraction of proviral cells are expressing HTLV-I [3].

CTLs replicate in response to the presence of proviral cells. So, we would expect the expression for the CTL response function to depend on y. Moreover, since replication of CTLs is done by mitosis then we would expect the CTL response function, $\mathcal{F}$, to also depend on z. The model proposed by Horatio Gomez-Acevedo, Li, and Jacobson (*unpublished*) [9] chooses the density-dependent (in z) expression $\nu\mathcal{F}(y,z) = \nu\frac{yz}{z+a}$ for the CTL response function. The constant ν is the responsiveness of the CTL response. For fixed y, $z = a$ is the number of CTLs required for the response to be at half maximum. This type of function is also called a Holling type II response [28] and is commonly used in modelling predator-prey systems.

Natural death is given by the constant per capita rates μ_1, μ_2, and μ_3 for healthy CD4$^+$ T-cells, proviral CD4$^+$ T-cells, and CTLs, respectively.

The global dynamics of (1.4.3) depends on the value of the basic reproductive numbers for HTLV-I and for the CTL response, R_0 and R_1, respectively. Depending on the value of these parameters there are between one and three equilibria. These three equilibria are $P_0 = (\frac{\lambda}{\mu_1}, 0, 0)$, $P_1 = (\bar{x}, \bar{y}, 0)$, and $P_2 = (x^*, y^*, z^*)$, where $\bar{x}$, $\bar{y}$, x^*, y^*, and z^* are all positive. We call P_0 the disease-free equilibrium, P_1 the carrier equilibrium, and P_2 the endemic equilibrium. In keeping with the interpretation above, P_1 is thought to be associated with asymptomatic carriers of HTLV-I. Similarly, P_2 is thought to be associated with HAM/TSP patients. One of these equilibria is asymptotically stable on the interior of the feasible region, Γ, depending on the values of R_0 and R_1. We summarize the results regarding the existence and stability of these

equilibria in Table 1.1.

Threshold Value	Equilibria		
	P_0	P_1	P_2
$R_1 < R_0 < 1$	GAS[1]	DNE[2]	DNE
$R_1 < 1 < R_0$	Unstable	GAS	DNE
$1 < R_1 < R_0$	Unstable	Unstable	GAS

Table 1.1: Summary of GLJ Model

1.4.2 Wodarz and Bangham (2000) [32]

A simple model which includes mitosis of healthy $CD4^+$ is proposed in Wodarz and Bangham (2000) [32]. Their model, which is an extension of the flow diagram (1.4.2), follows below.

$$\dot{x} = (\lambda + rxy)\left(1 - \frac{x+y}{k}\right) - \beta xy - \mu_1 x \tag{1.4.4a}$$

$$\dot{y} = \beta xy - \gamma yz - \mu_2 y \tag{1.4.4b}$$

$$\dot{z} = \nu y - \mu_3 z. \tag{1.4.4c}$$

Wodarz and Bangham (2000) [32] report the presence of a disease-free equilibrium, E_1, and of an endemic equilibrium, E_2. As with the previous model, an expression for the basic reproductive number, R_0, is determined. They then identify parameters where E_1 is stable and E_2 is unstable, where E_1 is unstable and E_2 is stable, and where both E_1 and E_2 are stable. When both E_1 and E_2 are stable we say that the model exhibits bistability. Clearly, if E_1 and E_2 are both stable then the limiting behaviour is dependent on the initial conditions.

[1] Globally Asymptotically Stable. By this we mean asymptotically stable within the interior of Γ.

[2] Does Not Exist.

Although the phenomenon of bistability is intuitively reasonable, it is rare in models of HTLV-I infection. Nevertheless, it has some interesting consequences. For example, under the appropriate conditions there can be persistence of HTLV-I infection when $R_0 < 1$.

1.4.3 Wodarz, Nowak, and Bangham (1999) [33]

It is possible to include terms representing mitotic division of both healthy and proviral $CD4^+$ T-cells [32, 33]. This was done by Wodarz, Nowak, and Bangham (1999) [33]. Their model is an extension the basic transfer diagram (1.4.2) and follows below.

$$\dot{x} = (\lambda + rx)\left(1 - \frac{x+y}{k}\right) - \beta xy - \mu_1 x \tag{1.4.5a}$$

$$\dot{y} = \beta xy + sy\left(1 \pm \frac{z+y}{k}\right) \pm \gamma yz \pm \mu_2 y \tag{1.4.5b}$$

$$\dot{z} = \nu \frac{yz}{z+1} - \mu_3 z. \tag{1.4.5c}$$

This model fails to exhibit bistability, however, it does express some interesting behaviour. In particular, this model undergoes a super-critical Hopf bifurcation resulting in the creation of a stable periodic orbit. The existence of a stable periodic orbit is invoked by the authors to explain data showing rapid oscillations in the proviral load of an individual with HTLV-I undergoing anit-retroviral treatment.

The ability of this model to explain sustained oscillations is significant because oscillations observed in patients with HTLV-I [33] is a specific example of a more general phenomenon [29]. Two other specific instances where oscillations are observed in the dynamics of the immune system are autoimmune disorders [17] and cancers [23].

The model we propose in the next section builds on the work done by Gomez-Acevedo, Li, and Jacobson (*unpublished*) [9]. As we shall see, modifying this model by altering the response function results in both periodic solutions and bistability. After a thorough analysis, we consider results of our model and compare them to the models discussed above.

1.5 Our Model

Our goal is to investigate the importance of the CTL response to the dynamics of HTLV-I infection. This is most easily done by altering the CTL response function, $\mathcal{F}(y,z)$. Since our focus remains on the immune response, we simplify our analysis by omitting the mitosis of healthy and proviral $CD4^+$ T-cells, despite strong evidence that mitosis is important to the persistence of infection and the development of disease [3, 5]. We therefore propose to amend the model of Gomez-Acevedo, Li, and Jacobson (*unpublished*) [9] by changing the response function. In order to easily distinguish our model from previous ones we will denote our response function by $F(y,z)$ instead of $\mathcal{F}(y,z)$.

Which response function is the most appropriate is currently unknown. Some well studied phenomena, such as antigen-induced cell death, give reason to suspect that the CTL response should become saturated after some density of CTLs. This condition is certainly satisfied by $\mathcal{F}(y,z) = \frac{yz}{z+a}$. However, $\mathcal{F}(y,z) = \frac{yz}{z+a}$ is hardly the only function which satisfies this condition. Since we do not know which function is the most appropriate, it would be desirable to choose $F(y,z)$ to be as general as possible. It is also desirable to choose $F(y,z)$ so that our results may be easily compared to previous models. We satisfy these conditions by choosing

$$F(y,z) = \frac{yz^n}{z^n + a} \tag{1.5.1}$$

where $n \in \mathbb{N}$ and $n \geq 2$. So, our model is written as

$$\dot{x} = \lambda - \mu_1 x - \beta xy \tag{M$_1$}$$

$$\dot{y} = \sigma\beta xy - \mu_2 y - \gamma yz \tag{M$_2$}$$

$$\dot{z} = \nu \frac{yz^n}{z^n + a} - \mu_3 z. \tag{M$_3$}$$

We further justify our choice of $F(y, z) = \frac{yz^n}{z^n+a}$ by noting that this family of functions has been used in immunological [17] and ecological [28] models. The findings of Iwami et al (2007) [17] deserve particular mention as their results provide an excellent justification for our choice of $F(y, z)$.

Iwami et al (2007) [17] proposes and analyzes a three compartment model of a general autoimmune disorder and investigates several different options for modelling the replication of CTLs as well as the cells targeted by the CTLs. One of the CTL response functions they investigated was $\mathcal{F}(y, z) = \frac{yz^2}{z^2+a}$. Use of this response function allowed them to provide important insights into previously unexplained phenomena such as tolerance, flare-up, and dormancy.

We now have a sufficient motivation and introduction to proceed with the analysis of our model, which is divided into two parts. In Chapter 2 we explore results which we are able to prove. Unfortunately, the response function we have chosen, $F(y, z) = \frac{yz^n}{z^n+a}$, limits the number of results we can prove analytically. Thus, in Chapter 3 we review some numerical results obtained by simulation in MATLAB and XPPAUT.

Chapter 2

Analytical Results

2.1 Feasible Region

Let $\mathbb{R}^3_+$ denote the positive octant of $\mathbb{R}^3$. Define

$$\Gamma = \left\{ (x, y, z) \in \mathbb{R}^3_+ : x \leq \frac{\lambda}{\mu_1}, x + y \leq \frac{\lambda}{\bar{m}}, z \leq \frac{\lambda\nu}{\bar{m}\mu_3} \right\},$$

where $\bar{m} = \min\{\mu_1, \mu_2\}$. In our first result, we show that Γ is the feasible region for this model.

Theorem 2.1.1 ***Region of Interest***

The system of ordinary differential equations (M) *is positively invariant in* Γ. *Moreover, in order to study the limiting behaviour of* (M) *in* $\mathbb{R}^3_+$ *it suffices to study* (M) *in* Γ.

Proof: It can be verified from (M) that $\mathbb{R}^3_+$ is positively invariant. Since populations of cells are non-negative quantities, we restrict any further analysis of this model to $\mathbb{R}^3_+$. From (M_1) we get

$$\dot{x} \leq \lambda - \mu_1 x \implies \begin{cases} \limsup_{t\to\infty} x(t) \leq \frac{\lambda}{\mu_1} & \\ \forall t > 0 : x(t) \leq \frac{\lambda}{\mu_1} & \text{if } x(0) \leq \frac{\lambda}{\mu_1} \end{cases}. \tag{2.1.1}$$

Similarly, we observe that adding (M_1) and (M_2) gives

$$(\dot{x}+\dot{y}) = \lambda + (\sigma-1)\beta xy - \mu_1 x - \mu_2 y - \gamma yz \leq \lambda - \bar{m}(x+y)$$
$$\implies \begin{cases} \limsup_{t\to\infty}(x(t)+y(t)) \leq \frac{\lambda}{\bar{m}} \\ \forall t>0 : x(t)+y(t) \leq \frac{\lambda}{\bar{m}} \qquad \text{if } x(0)+y(0) \leq \frac{\lambda}{\bar{m}} \end{cases}. \tag{2.1.2}$$

From equations (2.1.1) and (2.1.2) we may restrict our analysis to the region

$$\bar{\Gamma} = \left\{ (x,y,z) : (x,y,z) \in \mathbb{R}^3_+, x \leq \frac{\lambda}{\mu_1}, x+y \leq \frac{\lambda}{\bar{m}} \right\}.$$

(M_3) now yields

$$\dot{z} = \nu \underbrace{\frac{z^2}{z^2+a}}_{\leq 1} y - \mu_3 z \leq \nu(x+y) - \mu_3 z \leq \frac{\nu\lambda}{\bar{m}} - \mu_3 z$$
$$\implies \begin{cases} \limsup_{t\to\infty} z(t) \leq \frac{\nu\lambda}{\bar{m}\mu_3} \\ \forall t>0 : z(t) \leq \frac{\nu\lambda}{\bar{m}\mu_3} \qquad \text{if } z(0) \leq \frac{\nu\lambda}{\bar{m}\mu_3} \end{cases}. \tag{2.1.3}$$

The desired results follow from (2.1.1)-(2.1.3).

□

We now restrict all further analysis to the region Γ. Next, we consider the existence and stability properties of the equilibria of (M).

2.2 Equilibria

In this section we show that (M) has between one and four equilibria. Before we prove our main result we define some useful quantities. Define

$$
\begin{aligned}
I &= \left(0, \frac{\mu_2}{\gamma}(R_0 - 1)\right), \\
R_0 &= \frac{\lambda\sigma\beta}{\mu_1\mu_2}, \\
g(z) &= \beta\mu_3\gamma z^{n+1} + (\nu\mu_1\gamma + \beta\mu_2\mu_3)z^n - \nu(\lambda\sigma\beta - \mu_1\mu_2)z^{n-1} \\
&\quad + a\beta\mu_3\gamma z + a\beta\mu_2\mu_3, \text{ and} \\
\phi^{\pm} &= -\frac{\nu\mu_1\gamma + \beta\mu_2\mu_3}{3\beta\mu_3\gamma} \\
&\quad \pm \frac{\sqrt{(\nu\mu_1\gamma + \beta\mu_2\mu_3)^2 - 3\beta\mu_3\gamma(a\beta\mu_3\gamma + \mu_1\mu_2\nu - \lambda\sigma\beta\nu)}}{3\beta\mu_3\gamma}.
\end{aligned}
$$

We are now ready for the main result of this section.

Theorem 2.2.1 ***Number of Equilibria***

Consider the system (M) *inside the positively invariant set* Γ. (M) *has at most four equilibria subject to the following conditions.*

(a) *There always exists a disease free equilibrium,*

$$P_0 = (\tilde{x}, 0, 0) = \left(\frac{\lambda}{\mu_1}, 0, 0\right).$$

(b) *If* $R_0 > 1$ *then there exists a carrier (CTL-free) equilibrium,*

$$P_1 = (\bar{x}, \bar{y}, 0) = \left(\frac{\mu_2}{\sigma\beta}, \frac{\lambda\sigma\beta - \mu_1\mu_2}{\beta\mu_2}, 0\right).$$

(c) *If* $R_0 > 1$ *and if* $\min_{\{z\in I\}} g(z) = 0$ *then there is one additional endemic equilibrium,*

$$P_2 = (x^*, y^*, z^*),$$

where $z^* > 0$ *and where* $x^* > 0$ *and* $y^* > 0$ *are given as functions of* z^*.

(d) *If* $R_0 > 1$ *and if* $\min_{\{z\in I\}} g(z) < 0$ *then there are two additional endemic*

equilibria,

$$P_2 = (x^*, y^*, z^*) \text{ and}$$
$$P_3 = (x_L^*, y_L^*, z_L^*),$$

where $z_L^* > z^* > 0$*, and where* $x^* > 0$ *(*$x_L^* > 0$*) and* $y^* > 0$ *(*$y_L^* > 0$*) are given as functions of* z^* *(*z_L^**).*

Remark: Number of Equilibria

1. The converse of statements (b), (c), and (d) in Theorem 2.2.1 can be shown to be true.

2. If $n = 2$ then $\min_{\{z \in I\}} g(z) = g(\phi^+)$.

Proof: From (2.1.1), (2.1.2), and (2.1.3) we have that any equilibria of (M) which lies in $\mathbb{R}^3_+$ must also lie in Γ. So, it suffices to perform our analysis in $\mathbb{R}^3_+$. In order to identify all the possible equilibria of (M) we consider the following set of equations and break our discussion into several cases.

$$0 = \dot{x} = \lambda - \mu_1 x - \beta xy \tag{2.2.1a}$$
$$0 = \dot{y} = \sigma\beta xy - \mu_2 y - \gamma yz \tag{2.2.1b}$$
$$0 = \dot{z} = \nu \frac{yz^n}{z^n + a} - \mu_3 z. \tag{2.2.1c}$$

Case (a): Observe that $P_0 \in \mathbb{R}^3_+$ is a solution to (2.2.1). Moreover, further inspection of (2.2.1) gives that P_0 is the unique solution to (2.2.1) with $y = z = 0$.

Case (b): Suppose that $R_0 > 1$. Observe that

$$P_1 = \left(\frac{\mu_2}{\sigma\beta}, \frac{\lambda\sigma\beta - \mu_1\mu_2}{\beta\mu_2}, 0 \right) = \left(\frac{\mu_2}{\sigma\beta}, \frac{\mu_1}{\beta}(R_0 - 1), 0 \right).$$

Thus, $P_1 \in \mathbb{R}^3_+$. Similarly to Case (a), careful consideration of (2.2.1) gives that P_1 is the unique solution to (2.2.1) with $y \neq z = 0$.

Case (c-d): Let $R_0 > 1$. Previous cases have identified all solutions to (2.2.1) with $z = 0$. Thus, any further equilibria must reside in $\mathbb{R}^3_+$ and have a non-empty CTL compartment. In other words, we seek solutions to (2.2.1) in $\mathbb{R}^3_+$ with $z > 0$.

Rearranging (2.2.1b) and (2.2.1a) yields

$$x = \frac{\mu_2 + \gamma z}{\sigma\beta} \text{ and} \tag{2.2.2a}$$

$$y = \frac{\lambda - \mu_1 x}{\beta x} = \frac{\lambda\sigma\beta - \mu_1\mu_2 - \mu_1\gamma z}{\beta\mu_2 + \beta\gamma z}, \tag{2.2.2b}$$

respectively. Substituting (2.2.2a) and (2.2.2b) into (2.2.1c) subsequently gives

$$0 = \nu \frac{z^n}{z^n + a} \frac{\lambda\sigma\beta - \mu_1\mu_2 - \mu_1\gamma z}{\beta\mu_2 + \beta\gamma z} - \mu_3 z. \tag{2.2.3}$$

Observe that equation (2.2.1c) together with $z > 0$ implies that $y > 0$. Similarly, equation (2.2.1a) together with $y > 0$ implies $x > 0$. So, in order to find solutions to (2.2.1) in $\mathbb{R}^3_+$ with $z > 0$ it suffices to find solutions to (2.2.3) with $z > 0$. This can be shown to be equivalent to finding the positive roots of the polynomial $g(z)$.

Since $z > 0 \implies y > 0$, equation (2.2.2b) gives that any positive roots of $g(z)$ must occur in I. Furthermore, it follows from $g(0) = a\beta\mu_2\mu_3 > 0$ and $g(z) \overset{z\to\infty}{\to} \infty$ that

$$\min_{z\in I} g(z) = 0 (< 0) \implies g(z) \text{ has at least one (two) positive roots.} \tag{2.2.4}$$

It now suffices to show that

$$\min_{z\in I} g(z) = 0(<0) \implies g(z) \text{ has at most one (two) positive roots.} \qquad (2.2.5)$$

Unfortunately, due to the difficulty of solving $g(z) = 0$ we are required to subdivide the remainder of this section into two cases: $n = 2$ and $n \geq 3$.

Case (c-d)-I, $n = 2$: Assume that $\min_{z\in I} g(z) \leq 0$. When $n = 2$ $g(z)$ becomes

$$g(z) = \underbrace{\beta\mu_3\gamma}_{c_4>0} z^3 + \underbrace{(\nu\mu_1\gamma + \beta\mu_2\mu_3)}_{c_3>0} z^2 + \underbrace{(a\beta\mu_3\gamma + \mu_1\mu_2\nu - \lambda\sigma\beta\nu)}_{\tilde{c}} z + \underbrace{a\beta\mu_2\mu_3}_{c_0>0}.$$

Observe that

$$\tilde{c} \geq 0 \implies \forall z > 0 : g(z) > 0$$

is a contradiction with $\min_{z\in I} g(z) \leq 0$. Thus, it must be that $\tilde{c} < 0$. It follows that the first derivative of $g(z)$,

$$g'(z) = 3c_4 z^2 + 2c_3 z + \tilde{c},$$

has one positive root, ϕ^+, and one negative root, ϕ^-, given by the quadratic equation.

$$\begin{aligned}\phi^{\pm} &= \frac{-2c_3 \pm 2\sqrt{c_3^2 - 3\tilde{c}c_4}}{6c_4} \\ &= -\frac{\nu\mu_1\gamma + \beta\mu_2\mu_3}{3\beta\mu_3\gamma} \\ &\quad \pm \frac{\sqrt{(\nu\mu_1\gamma + \beta\mu_2\mu_3)^2 - 3\beta\mu_3\gamma(a\beta\mu_3\gamma + \mu_1\mu_2\nu - \lambda\sigma\beta\nu)}}{3\beta\mu_3\gamma}.\end{aligned}$$

The second derivative of $g(z)$,

$$g''(z) = 6c_4 z + 2c_3,$$

has one negative root, $\Phi = -\frac{c_3}{3c_4}$. This is a sufficient amount of information to sketch $g(z)$, see Figure 2.1.

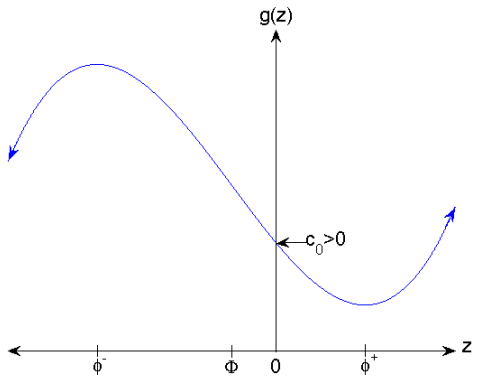

Figure 2.1: Sketch of $g(z)$ when $n = 2$ and $\min_{z\in I} g(z) \leq 0$.

The desired result follows from Figure 2.1.

Case (c-d)-II, $n \geq 3$: Again, we assume that $\min_{z\in I} g(z) \leq 0$. When $n \geq 3$ the function $g(z)$ becomes

$$g(z) = \underbrace{\beta\mu_3\gamma}_{c_4>0} z^{n+1} + \underbrace{(\nu\mu_1\gamma + \beta\mu_2\mu_3)}_{c_3>0} z^n + \underbrace{\nu\mu_1\mu_2(1-R_0)}_{c_2<0} z^{n-1} + \underbrace{a\beta\mu_3\gamma z}_{c_1>0} + \underbrace{a\beta\mu_2\mu_3}_{c_0>0}.$$

We now consider

$$\begin{aligned} g'(z) &= (n+1)c_4 z^n + nc_3 z^{n-1} + (n-1)c_2 z^{n-2} + c_1, \text{ and} \\ g''(z) &= n(n-1)z^{n-3}\left(\underbrace{\frac{n+1}{n-1}c_4 z^2 + c_3 z + \frac{n-2}{n}c_2}_{=p(z)}\right). \end{aligned}$$

The quadratic $p(z)$ has exactly one positive root, Ψ. It follows that Ψ is the unique positive root of $g''(z)$ and that $g'(z)$ can have at most two positive roots. However, since $\min_{z\in I} g(z) \leq 0$, $g(0) > 0$, $g'(0) > 0$, and $g(z) \overset{z\to\infty}{\to} \infty$, it also follows that $g'(z)$ must have at least two positive roots. We have now shown that $g'(z)$ has exactly two roots, ψ_1 and ψ_2. There is now sufficient information for a sketch of $g''(z)$, $g'(z)$, and $g(z)$, see Figure 2.2.

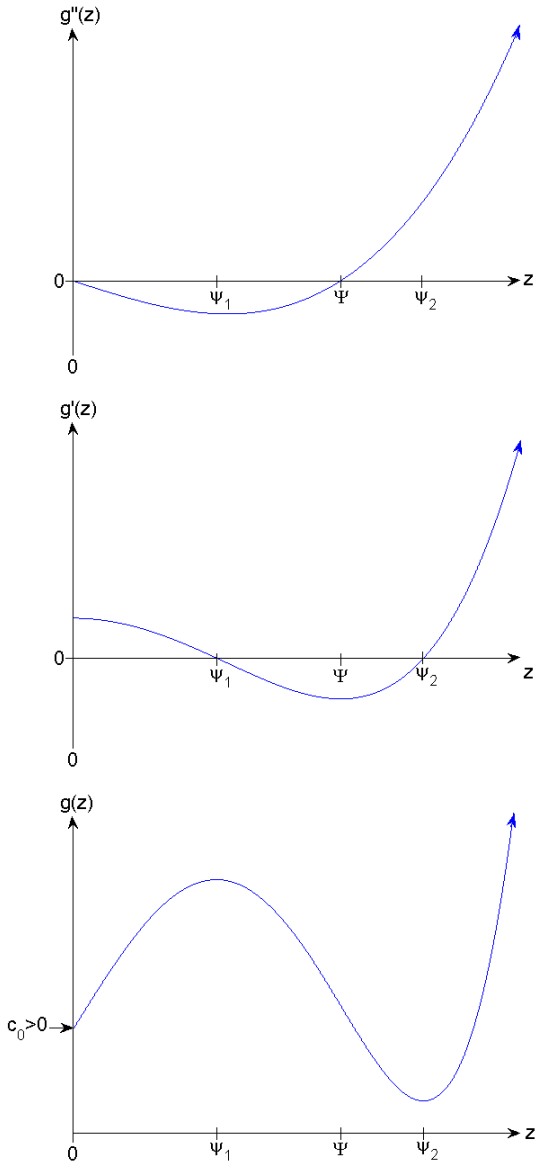

Figure 2.2: Sketch of $g''(z)$, $g'(z)$, and $g(z)$ when $n = 3$ and $\min_{z \in I} g(z) \leq 0$.

The desired result follows from Figure 2.2.

□

Due to the threshold qualities of R_0 we call this the basic reproduction number for HTLV-I. As in Gomez-Acevedo, Li, and Jacobson (*unpublished*) [9], R_0 determines the global stability properties of P_0. Unfortunately, our model differs from that of Gomez-Acevedo, Li, and Jacobson (*unpublished*) [9] in that R_0 no

longer determines the global stability properties of P_1. In the following section we further investigate the stability properties of the carrier equilibrium, P_1, and the endemic equilibria, P_2 and P_3.

2.3 Stability

We begin by exploring the stability of P_0 and P_1.

Theorem 2.3.1 ***Stability of*** P_0 ***and*** P_1

Consider the ordinary differential equations given by (M)*. Then,*

(a) P_0 *is globally asymptotically stable in* Γ *whenever* $R_0 \leq 1$ *and is unstable otherwise.*

(b) P_1 *exists and is locally asymptotically stable whenever* $R_0 > 1$ *and does not exist otherwise.*

Proof: Part (1): Suppose that $R_0 \leq 1$. Consider the Lyapunov function $V_0(x, y, z) = y$ for the equilibrium P_0. We now show that P_0 is globally asymptotically stable in Γ. Differentiating along the differential equations (M) yields

$$\begin{aligned}
\dot{V_0}(x, y, z) &= \sigma\beta xy - \mu_2 y - \gamma yz \\
&\leq (\sigma\beta x - \mu_2)y \\
&\leq \left(\frac{\lambda\sigma\beta}{\mu_1} - \mu_2\right) y \\
&= (R_0 - 1)\mu_2 y.
\end{aligned}$$

Where we used the fact that $(x, y, z) \in \Gamma \implies x \leq \frac{\lambda}{\mu_1}$.

It can be shown that the largest compact invariant set in $\{(x, y, z) \in \Gamma : \dot{V_0}(x, y, z) = 0\}$ is the singleton $\{P_0\}$. Thus, LaSalle's Invariance

Principle gives that P_0 is globally asymptotically stable.

Part (2): Suppose that $R_0 > 1$. We now consider the Jacobian matrix of (M), $J(x, y, z)$.

$$J(x,y,z) = \begin{bmatrix} -\mu_1 - \beta y & -\beta x & 0 \\ \sigma\beta y & \sigma\beta x - \mu_2 - \gamma z & -\gamma y \\ 0 & \frac{\nu z^n}{z^n + a} & \frac{an\nu y z^{n-1}}{(z^n+a)^2} - \mu_3 \end{bmatrix} \tag{2.3.1}$$

$$\implies J(P_0) = \begin{bmatrix} -\mu_1 & -\beta\tilde{x} & 0 \\ 0 & \sigma\beta\tilde{x} - \mu_2 & 0 \\ 0 & 0 & -\mu_3 \end{bmatrix}.$$

The eigenvalues of $J(P_0)$ are $-\mu_1$, $\sigma\beta\tilde{x} - \mu_2$, and $-\mu_3$. Thus, P_0 is unstable because

$$\sigma\beta\tilde{x} - \mu_2 = \mu_2(R_0 - 1) > 0.$$

We now evaluate $J(P_1)$.

$$J(P_1) = \begin{bmatrix} -\mu_1 - \beta\bar{y} & -\beta\bar{x} & 0 \\ \sigma\beta\bar{y} & 0 & -\gamma\bar{y} \\ 0 & 0 & -\mu_3 \end{bmatrix},$$

where we made use of $0 = \sigma\beta\bar{x}\bar{y} - \mu_2\bar{y}$. Next, we calculate the trace, determinant, and sum of principal minors, denoted by $\mathrm{tr}(J_{P_1})$, $\det(J_{P_1})$, and $\mathcal{M}(J_{P_1})$, respectively.

$$\begin{aligned}\mathrm{tr}(J_{P_1}) &= -(\mu_1 + \mu_3 + \beta\bar{y}) < 0\\ \det(J_{P_1}) &= -\sigma\beta^2\mu_3\bar{x}\bar{y} < 0\\ \mathcal{M}(J_{P_1}) &= \sigma\beta^2\bar{x}\bar{y} + \mu_1\mu_3 + \beta\mu_3\bar{y}\end{aligned}$$

Observe that

$$[\mathcal{M}\cdot\mathrm{tr} - \det](J_{P_1}) = -(\mu_1 + \beta\bar{y})(\sigma\beta^2\bar{x}\bar{y} + \mu_1\mu_3 + \beta\mu_3\bar{y}) < 0.$$

We now conclude by the Routh Hurwitz conditions that P_1 is locally asymptotically stable.

□

We now completely understand the global stability properties of P_0 and the local stability properties of P_1. As such, from now on we will assume that, unless otherwise stated, $R_0 > 1$.

A logical follow-up to Theorem 2.3.1 is to ask under what conditions, if any, is the equilibrium P_1 globally asymptotically stable. Unfortunately, it can be shown by solving (M) explicitly that all solutions in the plane $y = 0$ tend to P_0 asymptotically. In other words, P_1 can never be asymptotically stable in Γ. Since we wish to study HTLV-I infection, however, it is reasonable to exclude the plane $y = 0$ from consideration. Restricting our attention to $\Gamma \cap \{(x, y, z) \in \mathbb{R}^3 : y \neq 0\}$ now yields the following definition.

Definition: Global Asymptotic Stability of P_1

We say that P_1 is globally asymptotically stable if P_1 is asymptotically stable in $\Gamma \cap \{(x, y, z) \in \mathbb{R}^3 : y \neq 0\}$.

Following the above definition we are able to show that under certain circumstances P_1 is globally asymptotically stable. The following theorem formulates one particular result.

Theorem 2.3.2 ***Global Stability of*** P_1

Consider the differential equations given by (M). *Then* P_1 *is globally asymptotically stable, provided that*

$$a \geq (n-1)^{n-1} \left(\frac{\nu \bar{y}}{\mu_3 n} \right)^n . \tag{2.3.2}$$

Proof: Observe that the vector field generated by (M) in the region $\Gamma \cap \{(x, y, z) \in \mathbb{R}^3 : x = 0, y \neq 0\}$ points toward the interior of Γ. Thus, in order to show asymptotic stability in $\Gamma \cap \{(x, y, z) \in \mathbb{R}^3 : y \neq 0\}$ it suffices to show asymptotic stability in

$$A = \Gamma \cap \{(x, y, z) \in \mathbb{R}^3 : xy \neq 0\}.$$

Restricting ourselves to this case allows us to apply the Lyapunov function

$$V_1(x, y, z) = x - \bar{x} \ln x + \frac{1}{\sigma}(y - \bar{y} \ln y) + \frac{\gamma \bar{y}}{\sigma \mu_3} z.$$

Differentiation along the differential equations (M) yields

$$
\begin{aligned}
\dot{V}_1 &= \left(1-\frac{\bar{x}}{x}\right)\Big(\underbrace{\lambda}_{=\beta\bar{x}\bar{y}-\mu_1\bar{x}} - \beta xy - \mu_1 x\Big) \\
&\quad + \frac{1}{\sigma}\left(1-\frac{\bar{y}}{y}\right)(\sigma\beta xy - \underbrace{\mu_2}_{=\sigma\beta\bar{x}}\, y - \gamma yz) + \frac{\gamma\bar{y}}{\sigma\mu_3}\left(\frac{\nu y z^n}{z^n+a} - \mu_3 z\right) \\
&= \left(\beta\bar{x}\bar{y} + \mu_1\bar{x} - \beta xy - \mu_1 x - \beta\frac{\bar{x}^2\bar{y}}{x} - \mu_1\frac{\bar{x}^2}{x} + \beta\bar{x}y + \mu_1\bar{x}\right) \\
&\quad + \left(\beta xy - \beta\bar{x}y - \frac{\gamma}{\sigma}yz - \beta x\bar{y} + \beta\bar{x}\bar{y} + \frac{\gamma}{\sigma}\bar{y}z\right) \\
&\quad + \frac{\gamma\bar{y}}{\sigma\mu_3\nu}\frac{yz^n}{z^n+a} - \frac{\gamma}{\sigma}\bar{y}z \\
&= (\beta\bar{x}\bar{y} + \mu_1\bar{x})\left(2 - \frac{\bar{x}}{x} - \frac{x}{\bar{x}}\right) + \frac{\gamma yz}{\sigma}\left(-z^n + \frac{\nu\bar{y}}{\mu_3}z^{n-1} - a\right).
\end{aligned}
$$

The methods of optimization for single variable calculus now give that

$$
\left(2 - \frac{\bar{x}}{x} - \frac{x}{\bar{x}}\right)\begin{cases} = 0 & \text{if } x = \bar{x} \\ < 0 & \text{if } \bar{x} \neq x > 0 \end{cases} \quad \text{and}
$$

$$
\forall z \geq 0 : -z^n + \frac{\nu\bar{y}}{\mu_3}z^{n-1} - a \leq (n-1)^{n-1}\left(\frac{\nu\bar{y}}{\mu_3 n}\right)^n - a.
$$

Thus, (2.3.2) implies that $\forall (x,y,z) \in A : \dot{V}(x,y,z) \leq 0$. It can be shown that the largest compact invariant set in $\{(x,y,z) \in A : \dot{V}(x,y,z) = 0\}$ is $\{P_1\}$. LaSalle's Invariance Principle now gives that P_1 is asymptotically stable in A and our proof is complete.

□

If P_1 is globally asymptotically stable then the system (M) must have exactly two equilibria, P_0 and P_1 (i.e. $\min_{\{z\in I\}} g(z) > 0$). Certainly this is the case when (2.3.2) holds because (2.3.2) implies that $\forall z > 0$:

$$
\begin{aligned}
0 &\geq -z^n + \frac{\nu\bar{y}}{\mu_3} z^{n-1} - a \\
&> -\frac{\gamma}{\mu_2} z^{n+1} - (\frac{\nu\gamma\mu_1}{\beta\mu_2\mu_3} + 1) z^n \\
&\quad + \frac{\nu}{\beta\mu_2\mu_3}(\lambda\sigma\beta - \mu_1\mu_2) z^{n-1} - a\frac{\gamma}{\mu_2} z - a \\
&= -\frac{1}{\beta\mu_2\mu_3} g(z) \\
&\implies \min_{\{z\in I\}} g(z) > 0.
\end{aligned}
$$

This leads us to wonder whether the converse is also true. Indeed, although it seems entirely reasonable that $\min_{\{z\in I\}} g(z) > 0$ should imply the global asymptotic stability of P_1, this statement remains conjecture.

We now move onto the stability properties of P_2 and P_3, assuming of course that they exist.

Theorem 2.3.3 ***Stability of*** P_2 ***and*** P_3

If $an - a - z^{*n} < 0$ *then* P_2 *is locally asymptotically stable. Similarly, if* $an - a - z_L^{*n} < 0$ *then* P_3 *is locally asymptotically stable.*

Proof: The proofs for P_2 and P_3 are identical, so we will only consider the proof for the equilibrium P_2. We recall the Jacobian given in equation (2.3.1) and evaluate it at P_2. This gives

$$
\begin{aligned}
J(P_2) &= \begin{bmatrix} -\mu_1 - \beta y^* & -\beta x^* & 0 \\ \sigma\beta y^* & 0 & -\gamma y^* \\ 0 & \nu\frac{z^{*n}}{z^{*n}+a} & \frac{an\nu y^* z^{*n}}{(z^{*n}+a)^2} - \mu_3 \end{bmatrix} \\
&= \begin{bmatrix} -\frac{\lambda\sigma\beta}{\mu_2+\gamma z^*} & -\beta x^* & 0 \\ \sigma\beta y^* & 0 & -\gamma y^* \\ 0 & \frac{\mu_3 z^*}{y^*} & \frac{\mu_3(an-a-z^{*n})}{z^{*n}+a} \end{bmatrix},
\end{aligned}
$$

where we made use of the relationships (2.2.2a), (2.2.2b), as well as

$$0 = \sigma\beta x^* - \mu_2 - \gamma z^*, \text{ and}$$
$$0 = \frac{\nu y^* z^*}{z^{*n} + a} - \mu_3 z^*.$$

We can now calculate the determinant, trace, and sum of principle minors of $J(P_2)$.

$$\det(J_{P_2}) = -\frac{\lambda\sigma\beta\mu_3\gamma z^*}{\mu_2 + \gamma z^*} + \frac{\sigma\beta^2\mu_3 x^* y^*(an - a - z^{*n})}{z^{*n} + a} \tag{2.3.3a}$$
$$\operatorname{tr}(J_{P_2}) = -\frac{\lambda\sigma\beta}{\mu_2 + \gamma z^*} + \frac{\mu_3(an - a - z^{*n})}{z^{*n} + a} \tag{2.3.3b}$$
$$\mathcal{M}(J_{P_2}) = +\sigma\beta^2 x^* y^* - \frac{\lambda\sigma\beta\mu_3(an - a - z^{*n})}{(\mu_2 + \gamma z^*)(z^{*n} + a)} + \gamma\mu_3 z^*.$$

Next we calculate $[\mathcal{M} \cdot \operatorname{tr} - \det](J_{P_2})$.

$$\begin{aligned}
&[\mathcal{M} \cdot \operatorname{tr} - \det](J_{P_2}) \\
&\quad = -\frac{\lambda\sigma\beta \cdot \sigma\beta^2 x^* y^*}{\mu_2 + \gamma z^*} + \frac{(\lambda\sigma\beta)^2\mu_3(an - a - z^{*n})}{(\mu_2 + \gamma z^*)^2(z^{*n} + a)} \\
&\qquad + \frac{\sigma\beta^2 x^* y^*\mu_3(an - a - z^{*n})}{z^{*n} + a} - \frac{\lambda\sigma\beta\gamma\mu_3 z^*}{\mu_2 + \gamma z^*} \\
&\qquad + \frac{\gamma\mu_3^2 z^*(an - a - z^{*n})}{z^{*n} + a} - \frac{\lambda\sigma\beta\mu_3^2(an - a - z^{*n})^2}{(\mu_2 + \gamma z^*)(z^{*n} + a)^2} \\
&\qquad + \frac{\lambda\sigma\beta\gamma\mu_3 z^*}{\mu_2 + \gamma z^*} - \frac{\sigma\beta^2 x^* y^*\mu_3(an - a - z^{*n})}{z^{*n} + a} \\
&\quad = -\frac{\lambda\sigma\beta \cdot \sigma\beta^2 x^* y^*}{\mu_2 + \gamma z^*} + \frac{(\lambda\sigma\beta)^2\mu_3(an - a - z^{*n})}{(\mu_2 + \gamma z^*)^2(z^{*n} + a)} \\
&\qquad - \frac{\lambda\sigma\beta\mu_3^2(an - a - z^{*n})^2}{(\mu_2 + \gamma z^*)(z^{*n} + a)^2} + \frac{\gamma\mu_3^2 z^*(an - a - z^{*n})}{z^{*n} + a}. \qquad (2.3.3c) \\
&\quad < 0
\end{aligned}$$

Applying the Routh-Hurwitz criteria now yields the desired result.

□

Determining the stability of P_2 and P_3 in general is very difficult. Nevertheless, it is possible to prove that the equilibrium P_3 undergoes a Hopf bifurcation with respect to the parameter ν. Before proving this result, however, we must consider the following lemma.

Lemma 2.3.4 ***z_L^* as a function of ν***

Consider the system of ordinary differential equations given by (M)*. Fix all parameters other than ν. Then there exists some $\bar{\nu} > 0$ such that $\min_{\{z \in I\}} g(z) = 0$ when $\nu = \bar{\nu}$ and $\min_{\{z \in I\}} g(z) < 0$ when $\nu > \bar{\nu}$. Moreover, z^* is a continuous monotonically decreasing function of ν and z_L^* is a continuous monotonically increasing function of ν such that*

$$
\begin{aligned}
&z_L^* \overset{\nu \to \infty}{\to} \frac{\lambda\sigma\beta - \mu_1\mu_2}{\mu_1\gamma} = \frac{\mu_2}{\gamma}(R_0 - 1),\\
&z^* \overset{\nu \to \infty}{\to} 0,\\
&z^* \overset{\nu \to \bar{\nu}^-}{\to} z^*|_{\nu=\bar{\nu}}, \text{ and}\\
&z_L^* \overset{\nu \to \bar{\nu}^+}{\to} z^*|_{\nu=\bar{\nu}}.
\end{aligned}
$$

Proof: We begin by observing that determining the positive roots of $g(z)$ is equivalent to finding the positive intersections of the functions $f(z)$ and $h(z)$, given below.

$$
\begin{aligned}
f(z) &= \frac{z^n}{z^n + a},\\
h(z) &= \frac{\beta\mu_3}{\nu} \frac{\mu_2 z + \gamma z^2}{\lambda\sigma\beta - \mu_1\mu_2 - \mu_1\gamma z}.
\end{aligned}
$$

From Theorem 2.2.1 we know that $f(z)$ and $h(z)$ can have at most two positive intersections and that these intersections occur in the interval I. We now restrict ourselves to this interval and draw a quick sketch of $f(z)$ and $h(z)$ for various values of ν, see Figure 2.3.

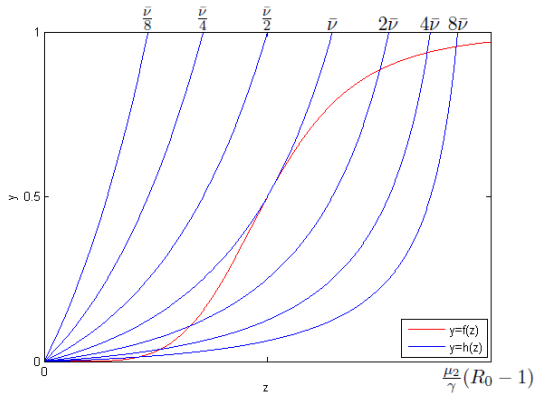

Figure 2.3: The functions $f(z)$ and $h(z)$ for various values of ν.

Figure 2.3 makes the behaviours of $h(z)$ and $f(z)$ clear. This gives us the desired results.

□

To emphasize the dependence of z^* and z_L^* on ν we sometimes use the notation $z^* = z^*(\nu)$ and $z_L^* = z_L^*(\nu)$. Similarly, we will sometimes write $P_2 = P_2(\nu)$ and $P_3 = P_3(\nu)$.

In order to state the next theorem it is convenient to define the terms ξ, $\hat{\nu}$, and $\tilde{\nu}$. We denote by ξ the unique positive root of the quadratic polynomial

$$\rho(z) = z^2 - \frac{\mu_2}{\gamma}\left(\frac{n-1}{n}R_0 - 2\right)z - \frac{\mu_2^2}{\gamma^2}(R_0 - 1).$$

Lemma 2.3.4 gives that if $\xi < \frac{\mu_2}{\gamma}(R_0 - 1)$ then there exists some $\hat{\nu} > \bar{\nu}$ such that

$$\forall \nu > \hat{\nu} : z_L^*(\nu) > \xi \implies \rho(z_L^*(\nu)) > 0. \tag{2.3.4}$$

Similarly, we note that if $\sqrt[n]{an-a} < \frac{\mu_2}{\gamma}(R_0-1)$ then $\exists \tilde{\nu} > \bar{\nu}$ such that $\forall \nu > \tilde{\nu}$: $z_L^*(\nu) > \sqrt[n]{an-a}$.

Theorem 2.3.5 ***Hopf Bifurcation***

Consider the system (M)*. Suppose that this system satisfies the following criteria.*

$$\frac{\mu_3 n}{\mu_1} \leq 1, \tag{2.3.5a}$$

$$\xi < \frac{\mu_2}{\gamma}(R_0-1), \tag{2.3.5b}$$

$$\sqrt[n]{an-a} < \frac{\mu_2}{\gamma}(R_0-1), \textit{and} \tag{2.3.5c}$$

$$0 < [\mathcal{M} \cdot tr - \det](J_{P_3(\hat{\nu})}) \tag{2.3.5d}$$

Then the equilibrium $P_3 = (x_L^*, y_L^*, z_L^*)$ undergoes a Hopf bifurcation for some $\nu \in (\hat{\nu}, \infty)$.

Proof: In order to show that a Hopf bifurcation occurs with respect to $\nu \in (\hat{\nu}, \infty)$ it suffices to show the following.

(a) $\forall \nu > \hat{\nu}$: $\det(J_{P_3(\nu)}) < 0$ and $\mathrm{tr}(J_{P_3(\nu)}) < 0$.

(b) $[\mathcal{M} \cdot \mathrm{tr} - \det](J_{P_3(\nu)})$ changes sign at least once in $(\hat{\nu}, \infty)$.

Part (a): Suppose that $\nu > \hat{\nu}$. Recall that $z_L^* \in I$ implies $z_L^* < \frac{\lambda\beta\sigma - \mu_1\mu_2}{\gamma\mu_1}$. We use this as well as (2.3.5a) show that $\mathrm{tr}(J_{P_3}) < 0$.

$$\begin{aligned}
\mathrm{tr}(J_{P_3}) &= -\frac{\lambda\sigma\beta}{\mu_2+\gamma z_L^*} + \frac{\mu_3(an-a-{z_L^*}^n)}{{z_L^*}^n+a} \\
&< -\frac{\lambda\sigma\beta}{\mu_2+\gamma z_L^*} + \mu_3 n \\
&= \frac{\mu_3 n(\mu_2+\gamma z^*) - \lambda\sigma\beta}{\mu_2+\gamma z_L^*} \\
&< \frac{\mu_3 n\left(\mu_2 + \frac{\lambda\sigma\beta-\mu_1\mu_2}{\mu_1}\right) - \lambda\sigma\beta}{\mu_2+\gamma z_L^*} \\
&= \frac{\lambda\sigma\beta}{\mu_2+\gamma z_L^*}\left(\frac{\mu_3 n}{\mu_1} - 1\right) \\
&\leq 0.
\end{aligned}$$

Next, we use (2.3.4) and (2.3.5b) to show that $\det_{P_3(\nu)} < 0$.

$$\begin{aligned}
\det_{P_3(\nu)} &= -\frac{\lambda\sigma\beta\mu_3\gamma z_L^*}{\mu_2+\gamma z_L^*} + \frac{\sigma\beta^2 x_L^* y_L^* \mu_3(an-a-{z_L^*}^n)}{{z_L^*}^n+a} \\
&< -\frac{\lambda\sigma\beta\mu_3\gamma z_L^*}{\mu_2+\gamma z_L^*} + \sigma\beta^2 x_L^* y_L^* \mu_3 n \\
&= \frac{-\lambda\sigma\beta\mu_3\gamma z_L^* + \mu_3 n(\lambda\sigma\beta - \mu_1\mu_2 - \mu_1\gamma z_L^*)(\mu_2+\gamma z_L^*)}{\mu_2+\gamma z_L^*} \\
&= \frac{-\mu_1\mu_3 n\gamma^2\rho(z_L^*)}{\mu_2+z_L^*} \\
&< 0.
\end{aligned}$$

Part (b): We recall that $\forall\nu > \tilde{\nu} : z_L^*(\nu) > \sqrt[n]{an-a}$. From (2.3.3c) we have $\forall\nu > \tilde{\nu} : [\mathcal{M}\cdot\mathrm{tr} - \det](J_{P_3(\nu)}) < 0$. This, together with (2.3.5d), gives that $[\mathcal{M}\cdot\mathrm{tr} - \det](J_{P_3(\nu)})$ changes sign at least once in the interval $(\hat{\nu},\tilde{\nu}) \subset (\hat{\nu},\infty)$.

It now follows that P_3 undergoes a Hopf bifurcation with respect to ν in the desired interval.

□

We would like to show that there exist parameters which satisfy Theorem 2.3.5. Due to the complexity of some of the calculations, notably $[\mathcal{M} \cdot \mathrm{tr} - \det](J_{P_3})$, we will defer this part of the analysis to the next section.

Chapter 3

Numerical Results

In Chapter 2 we were able to prove a number of significant results. Of these results, two are critically important to the interpretation of our model. First, Theorem 2.3.1 together with Theorem 2.3.3 allows for the possibility that our model exhibits bistability (multistability) between a carrier equilibrium and one (or more) endemic equilibria. Second, Theorem 2.3.5 allows for the possibility of the existence of periodic solutions. Although we are able to identify conditions under which these phenomena would occur, it remains unclear whether there exist parameter values which satisfy these conditions. Moreover, in the case of Theorem 2.3.5 we are unsure of the nature of the Hopf bifurcation. Due to the complexity of this model, investigating these problems is best done using numerical methods.

In the following sections we use programs coded in MATLAB and XPPAUT to further investigate these two results. When applying these methods we observe bistability[1], stable and unstable periodic orbits. As we previously mentioned, the consequences of these results are of critical importance to the interpretation of the model. Indeed, this is the first model of HTLV-I to exhibit bistability of this nature. Moreover, this is also the first model of HTLV-I to exhibit unstable periodic solutions.

[1]Bistability is observed between P_1 and either P_3 or a locally asymptotically stable periodic solution

Finally, we adopt some realistic parameters from Gomez-Acevedo, Li, and Jacobson (*unpublished*) [9] and investigate the behaviour of this model. For these parameters bistability as well as both stable and unstable periodic solutions are all detected. This underscores the importance of these phenomena to our model.

3.1 Sub-Critical Hopf Bifurcation

We begin our numerical analysis with an investigation into the Hopf Bifurcation discussed in Theorem 2.3.5. In particular, we verify that there exist parameters which satisfy Theorem 2.3.5.

Theorem 3.1.1 ***Hopf Bifurcation II***

The system (M) *with parameters*

$$[\lambda, \beta, \sigma, \gamma, a, \mu_1, \mu_2, \mu_3, n] = \left[3, 1, \frac{1}{2}, \frac{1}{2}, \frac{9}{10}, 1, 1, \frac{1}{2}, 2\right]$$

undergoes a Hopf Bifurcation with respect to $\nu \in (5.27, \infty)$.

Proof: We would like to apply Theorem 2.3.5. We now verify conditions (2.3.5) numerically in MATLAB using the code given in "HBVerification.m"[2]. From "HBVerification.m" we were also able to determine that $\bar{\nu} \approx 5.27 < \hat{\nu}$. So, the system undergoes a Hopf Bifurcation with respect to $\nu \in (5.27, \infty)$. We use "bif.m" as well as "model.ode" to produce the following bifurcation diagram.

[2]For all M-files and ODE files, please see Appendix A

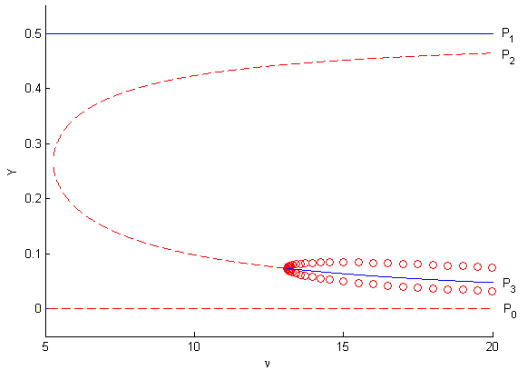

Figure 3.1: Bifurcation Diagram With Respect to ν.

□

We have demonstrated that there exist parameters which satisfy Theorem 2.3.5. Furthermore, as can be seen in Figure 3.1, the Hopf Bifurcation in Theorem 2.3.5 may result in an unstable periodic solution. Although it is not possible to do so numerically, we would like to show that this Hopf bifurcation is always sub-critical. It is possible, however, to demonstrate numerically that the conditions specified in Theorem 2.3.5 are sufficient but not necessary.

Proposition 3.1.2 (2.3.5) ***are not Necessary***

The conditions given in Theorem 2.3.5 under which (M) *undergoes a Hopf Bifurcation with respect to* ν *are sufficient but not necessary.*

Proof: We begin by considering the parameters

$$[\lambda, \beta, \sigma, \gamma, a, \mu_1, \mu_2, \mu_3, n] = \left[0.17, 1, \frac{1}{2}, 4, \frac{1}{100}, \frac{1}{100}, \frac{1}{10}, 1, 2\right]$$

These parameters do not satisfy (2.3.5a). From "HBVerification.m" we find that (2.3.5d) is also not satisfied. However, "bif.m" in MATLAB and "model.ode" in XPPAUT produce the bifurcation diagram Figure 3.2.

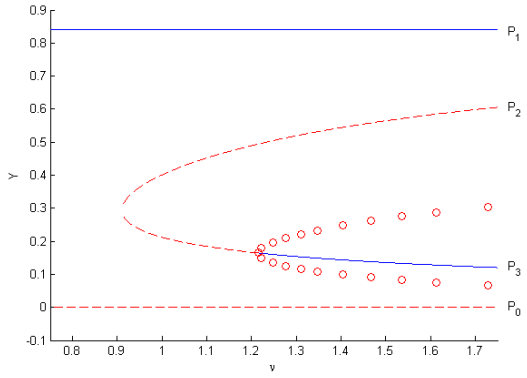

Figure 3.2: Bifurcation Diagram With Respect to ν.

□

This phenomenon is robust in the sense that we observe sub-critical Hopf bifurcations for the parameters λ, σ, β, γ, ν, a, μ_1, μ_2, and μ_3. Moreover, we observe a sub-critical Hopf bifurcation with respect to λ when $n = 3$.

Theorem 3.1.3 ***Hopf Bifurcation III***

When $n = 2$ (M) undergoes sub-critical Hopf bifurcations with respect to the parameters λ, σ, β, γ, ν, a, μ_1, μ_2, and μ_3. Moreover, when $n = 3$ there exists a sub-critical Hopf bifurcation with respect to λ.

Proof: Consider the parameters

$$[\lambda, \beta, \sigma, \gamma, \nu, a, \mu_1, \mu_2, \mu_3, n] = \left[0.17, 1, \frac{1}{2}, 4, 1, \frac{1}{100}, \frac{1}{100}, \frac{1}{10}, 1, 2\right] \tag{3.1.1}$$

A Hopf bifurcation occurs for each of the parameters λ, σ, β, γ, ν, a, μ_2, and μ_3. We have shown the Hopf bifurcation with respect to nu in Figure 3.2. The remaining bifurcation diagrams are constructed with "bif.m" in MATLAB as well as "model.ode" in XPPAUT, see Figure 3.3.

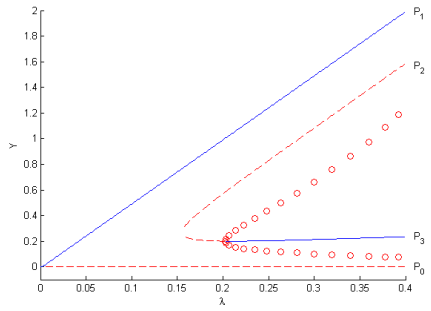

(a) λ

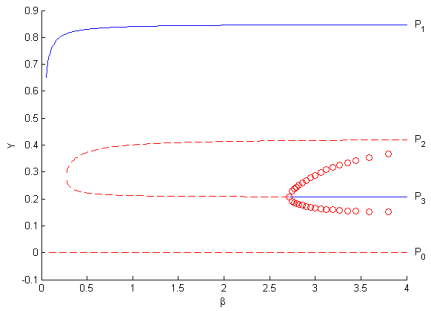

(b) β

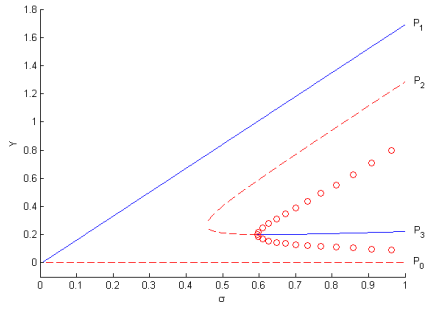

(c) σ

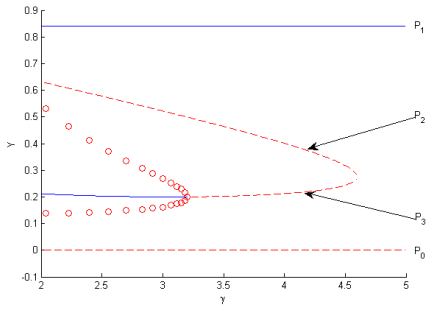

(d) γ

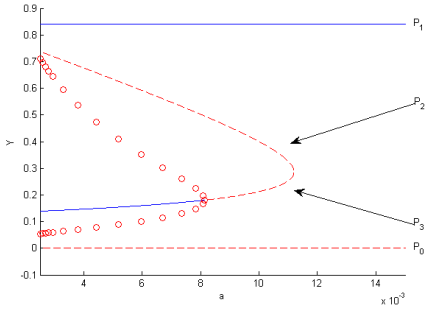

(e) a

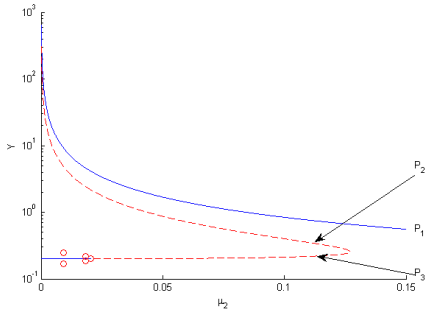

(f) μ_2

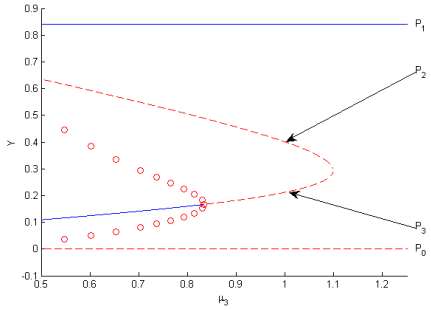

(g) μ_3

Figure 3.3: Bifurcation Diagrams with (3.1.1).

It is convenient to produce some graphs with logarithmic scales. We note that P_0 is necessarily omitted in the graphs where the scale of the Y-axis is logarithmic. Fortunately, this causes no difficulties, as the global behaviour of P_0 is completely understood.

Next we consider the parameters

$$[\lambda, \beta, \sigma, \gamma, \nu, a, \mu_1, \mu_2, \mu_3, n] = \left[0.5, 1, \frac{1}{2}, 4, 1, \frac{1}{100}, \frac{1}{100}, \frac{1}{10}, 1, 2\right]. \tag{3.1.2}$$

Under these parameters there is a Hopf bifurcation with respect to μ_1, as given by Figure 3.4.

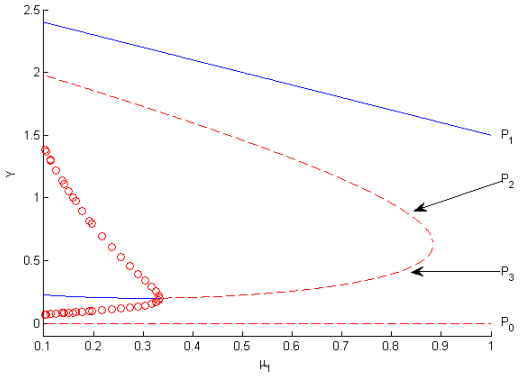

Figure 3.4: Bifurcation Digram with respect to μ_1 and with (3.1.2).

Finally, we consider the parameters

$$[\lambda, \beta, \sigma, \gamma, \nu, a, \mu_1, \mu_2, \mu_3, n] = \left[0.85, 1, \frac{1}{2}, 4, 1, \frac{1}{100}, \frac{1}{100}, \frac{1}{10}, 1, 3\right]. \tag{3.1.3}$$

Under these conditions there is a Hopf bifurcation with respect to λ, see Figure 3.5.

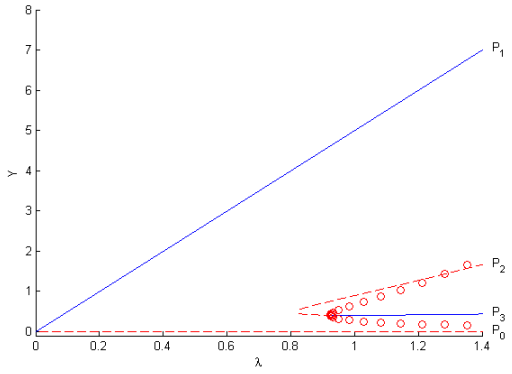

Figure 3.5: Bifurcation Diagram with (3.1.3)

□

Proposition 3.1.2 leads us to conjecture that sub-critical Hopf bifurcations occur for all values of n and with respect to all parameters. Unfortunately, we are unable to verify this numerically or otherwise.

It is tempting to simply ignore the unstable periodic orbits. Indeed, due to their instability we would not necessarily expect them to be of significant biological importance. As it turns out, however, behaviour of these unstable periodic orbits have a critical import on the interpretation of our model. Thus, we conclude this section with an investigation of solutions with initial conditions close to an unstable periodic orbit.

Theorem 3.1.4 ***Behaviour Near Unstable Periodic Orbit***

There are parameters for which there exists an unstable periodic solution satisfying the following properties.

(a) *Solutions with initial conditions near the unstable periodic orbit exhibit prolonged transient oscillations.*

(b) *Solutions exhibiting prolonged transient oscillations may converge to either P_1 and P_3.*

Solutions to this system with initial conditions near this unstable periodic orbit exhibit prolonged transient oscillations before converging to either P_1 or P_3.

Proof: We begin by considering the following parameters.

$$[\lambda, \beta, \sigma, \gamma, \nu, a, \mu_1, \mu_2, \mu_3, n] = [0.17, 1, 0.5, 4, 1, 0.01, 0.01, 0.01, 1, 2]. \tag{3.1.4}$$

Using XPPAUT we verify that for this set of parameters there exists an unstable periodic solution. Furthermore, XPPAUT gives us a set of initial conditions close to this periodic orbit.

$$(x_0, y_0, z_0) = (0.8243, 0.2424, 0.1081). \tag{3.1.5}$$

Using these initial conditions as a starting point we now investigate the behaviour of solutions in a neighbourhood of (x_0, y_0, z_0). We proceed by using the MATLAB code "pSolns.m".

The "pSolns.m" program considers the circle centered at (x_0, y_0, z_0) and perpendicular to the vectorfield (M)[3]. We select a number of evenly spaced points on this circle to serve as initial conditions for numerical solutions to (M). We are then able to identify which initial conditions converge to P_1 or to P_3. Finally, the code selects two sets of initial conditions on the circle, one of which converges to P_1 and one of which converges to P_3. These results are displayed in Figure 3.6 and Figure 3.7.

[3]The circle is perpendicular to (M) at (x_0, y_0, z_0) if the plane in which the circle lies is perpendicular to (M) at (x_0, y_0, z_0).

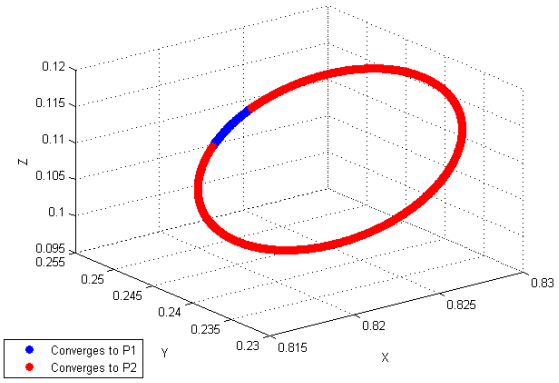

Figure 3.6: Convergence of Solutions with Initial Conditions close to the Periodic Orbit

(a) Solution Convergent to P_1

(b) Solution Convergent to P_3

Figure 3.7: Orbits with Transient Oscillations

Figure 3.6 shows that, as claimed, solutions do indeed converge to either P_1 or P_3. Figure 3.7 illustrates that there are solutions convergent to both P_1 and P_3 which exhibit prolonged transient oscillations.

□

Remark: Initial Conditions

It is interesting to note that the L_2 norm of the difference between the two sets of initial conditions used to produce Figure 3.7 is approximately 6×10^{-5}. Indeed, we conjecture that it is possible to find two sets of initial conditions which are arbitrarily close together such that both exhibit prolonged oscillations, one converges to P_1, and the other to P_3.

Using numerical methods, we have now come to a reasonable understanding of the sub-critical Hopf bifurcations present in (M). Interestingly, however, (M) is able to undergo not only sub-critical Hopf bifurcations but also super-critical Hopf bifurcations. The next section is dedicated to examining this behaviour.

3.2 Super-Critical Hopf Bifurcation

Further investigation of (M) quickly reveals a super-critical Hopf Bifurcation with respect to when $n = 2$.

Theorem 3.2.1 ***Super-Critical Hopf Bifurcation***

Suppose that $n = 2$. *The system* (M) *undergoes a super-critical Hopf bifurcation with respect to* λ, σ, β, γ, ν, a, μ_1, μ_2, *and* μ_3.

Proof: Consider the set parameters

$$[\lambda, \beta, \sigma, \gamma, a, \mu_1, \mu_2, \mu_3, n] = [2, 1, 1, 1.99, 0.45, 1, 1, 0.5, 2]. \tag{3.2.1}$$

Using "bif.m" and XPPAUT we produce Figures 3.8 and 3.9.

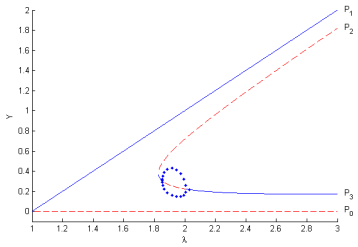

(a) λ

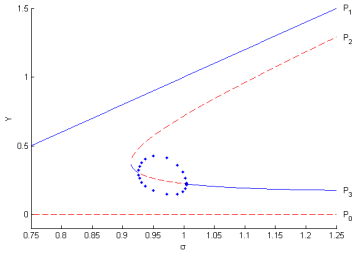

(b) σ

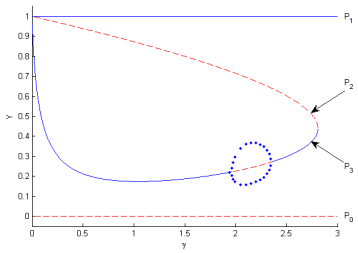

(c) γ

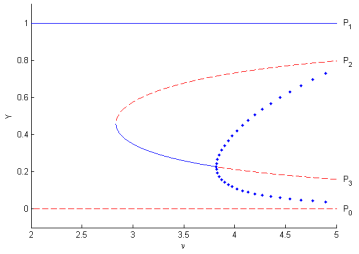

(d) ν

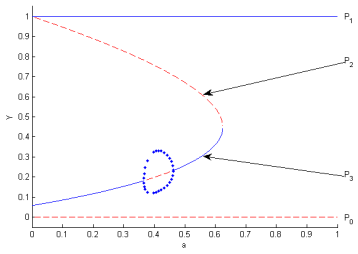

(e) a

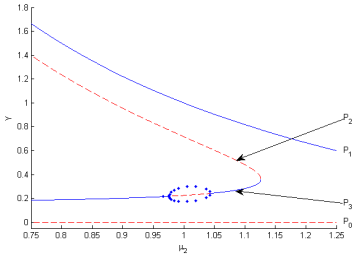

(f) μ_2

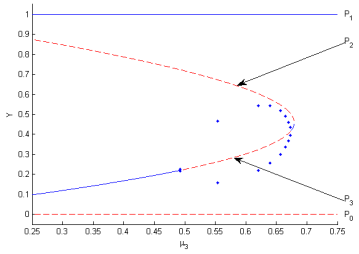

(g) μ_3

Figure 3.8: Bifurcation Diagrams with (3.2.1) and $\nu = 3.85$.

(a) β (b) μ_1

Figure 3.9: Bifurcation Diagrams with (3.2.1) and $\nu = 3.6$.

□

As in the previous section, we are able to find super-critical Hopf bifurcations when $n = 3$. The next theorem shows a super-critical Hopf bifurcation with respect to λ when $n = 3$.

Theorem 3.2.2 ***Super-Critical Hopf Bifurcation II***

Let $n = 3$. The system (M) *undergoes a super-critical Hopf bifurcation with respect to λ.*

Proof: Consider the following parameters.

$$[\lambda, \beta, \sigma, \gamma, \nu, a, \mu_1, \mu_2, \mu_3] = [2, 1, 1, 1.99, 3.26, 0.45, 1, 1, 0.5, 3]. \tag{3.2.2}$$

Using "bif.m" as well as XPPAUT yields Figure 3.10.

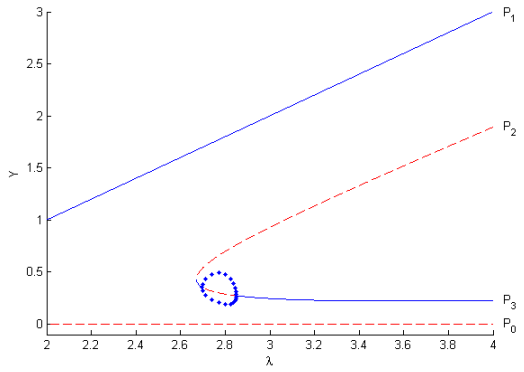

Figure 3.10: Bifurcation Diagram with (3.2.2)

□

We concluded the previous section by considering some solutions to (M). In this section we omit such a consideration. Alternatively, we choose to produce a number of simulations using realistic parameters derived in Gomez-Acevedo, Li, and Jacobson (*unpublished*) [9].

3.3 Realistic Parameters

In this section we examine (M) under realistic parameters. In particular, we show that for realistic parameters both sub- and super-critical Hopf bifurcation occur, and the model exhibits bistability. The parameters we will use were estimated in Gomez-Acevedo, Li, and Jacobson (*unpublished*) [9] and follow in Table 3.1.

Parameter	Value	Units
λ	20	cells mm^{-3} day^{-1}
β	0.001	mm^3 $cells^{-1}$ day^{-1}
σ	0.05	N/A
γ	0.2	mm^3 $cells^{-1}$ day^{-1}
μ_1	0.015	day^{-1}
μ_2	0.015	day^{-1}
μ_3	0.015	day^{-1}

Table 3.1: Estimation of Parameters

Gomez-Acevedo, Li, and Jacobson (*unpublished*) [9] took ν between 0.0001 and 0.0081 day^{-1}. Specifically, simulations performed used the values $\nu = 0.001$ day^{-1}, $\nu = 0.041$ day^{-1}, and $\nu = 0.081$ day^{-1}. We opt to choose $a = 1$ cell^{2n} mm^{-3n}. Although seemingly arbitrary, there is precedence for such a choice illustrated by the choice of $\mathcal{F}(y, z) = \frac{yz}{z+1}$ by both Wodarz, Nowak, and Bangham (1999) [33] and Gomez-Acevedo, Li, and Jacobson (*unpublished*) [9].

In our next theorem we show that a super-critical Hopf Bifurcation occurs with respect to λ when $n \in \{2, 3\}$ and $\nu \cdot \text{day} \in (0.001, 0.1)$.

Theorem 3.3.1 ***Super-Critical Hopf Bifurcation with Realistic Parameters***

Consider the system (M) *with parameters given in Table 3.1. If* $n \in \{2, 3\}$ *and* $\nu \cdot day \in (0.001, 0.081)$ *then this system undergoes a super-critical Hopf bifurcation with respect to* λ.

Proof: First we consider when $n = 2$. We proceed by constructing the two parameter bifurcation diagram, Figure 3.11, using the MATLAB M-file "bif2p.m". For ease of viewing we do not show the periodic orbits.

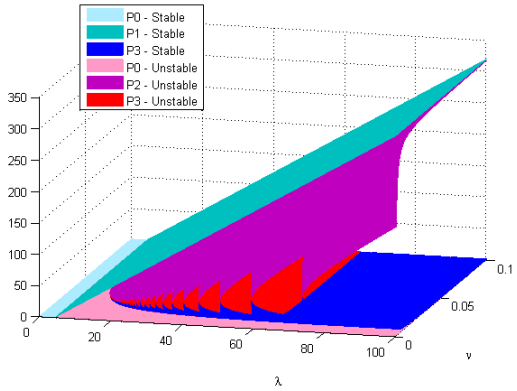

Figure 3.11: Bifurcation Diagram with Respect to λ and ν ($n = 2$).

Further investigation shows that only P_0 and P_3 undergo change in stability. Since the behaviour of P_0 is completely understood, it is useful to consider the surface in Figure 3.11 which represents P_3. We do this in Figure 3.12.

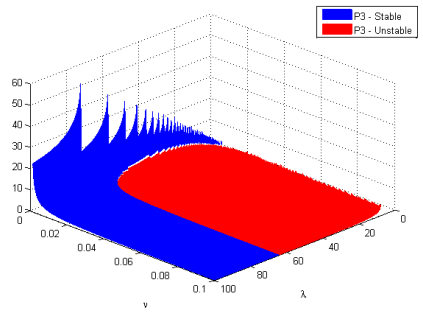

(a) Bifurcation Diagram Showing Equilibrium P_3 Only.

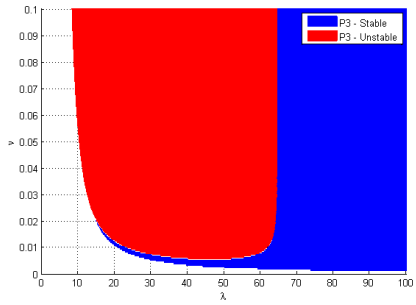

(b) Projection of P_3 into the λ-ν Plane.

Figure 3.12: Bifurcation Diagram with Respect to λ and ν, Showing P_3 Only.

It is clear from Figure 3.12 that a super-critical Hopf bifurcation occurs both with respect to λ and ν. For completeness of argument, we now show a λ-section and a ν-section of the bifurcation diagram Figure 3.11 showing the stable periodic orbits, see Figure 3.13. As above, we use the MATLAB code "bif.m". Limitations in XPPAUT prevent us from using this program to detect the stable periodic orbits. Fortunately, stable periodic orbits are easy to detect numerically and we use trial and error in MATLAB to do so.

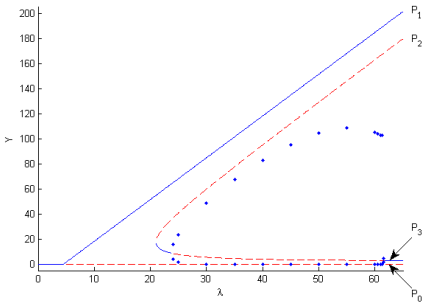

(a) λ-section with $\nu = 0.01$.

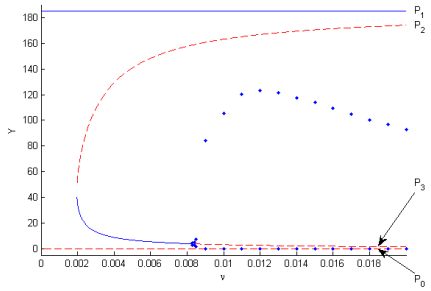

(b) ν-section with $\lambda = 60$.

Figure 3.13: Lambda and Nu Sections of Surface in Figure 3.11.

Next we consider when $n = 3$ and proceed by the same strategy as above.

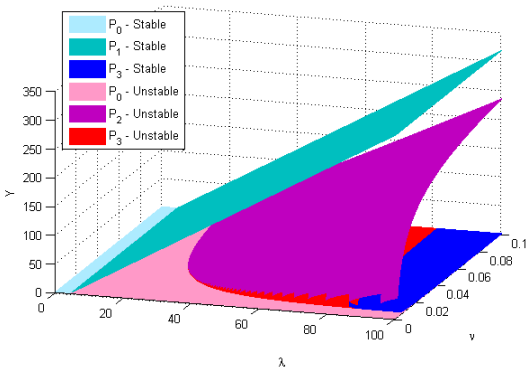

Figure 3.14: Bifurcation Diagram with Respect to λ and ν ($n = 3$).

As above, it is useful to consider the surface in Figure 3.14 which represents P_3.

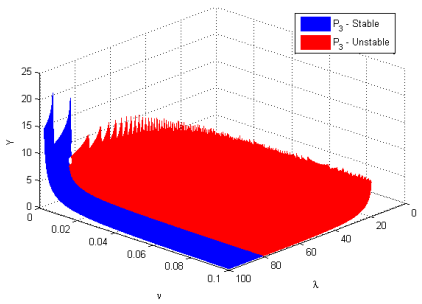

(a) Bifurcation Diagram Showing Equilibrium P_3 Only.

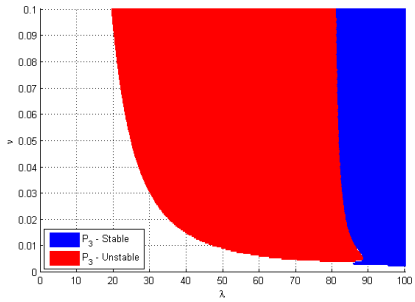

(b) Projection of P_3 into the λ-ν Plane.

Figure 3.15: Bifurcation Diagram with Respect to λ and ν ($n = 3$); P_3 Only.

For completeness we display a λ-section as well as a ν-section of Figure 3.14. Unfortunately, we were unable to detect the stable periodic orbits with either MATLAB or XPPAUT. Nevertheless, the existence of the desired Hopf bifurcation is clear.

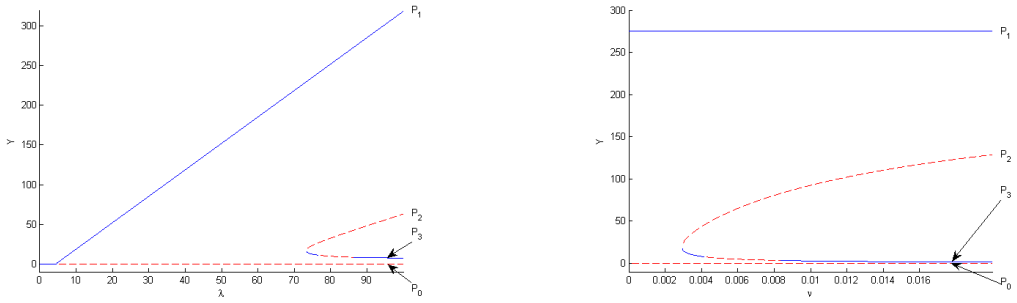

(a) λ-section with $\nu = 0.004$.

(b) ν-section with $\lambda = 87$.

Figure 3.16: Lambda and Nu Sections of Surface in Figure 3.14.

□

In the case where we can detect the stable periodic solution it is interesting to visualize these solutions. Below we solve (M) numerically with

$$\begin{aligned}&[\lambda, \beta, \sigma, \gamma, \nu, a, \mu_1, \mu_2, \mu_3, n] \\ &\quad = [35, 0.001, 0.05, 0.2, 0.01, 1, 0.015, 0.015, 0.015, 2].\end{aligned} \tag{3.3.1}$$

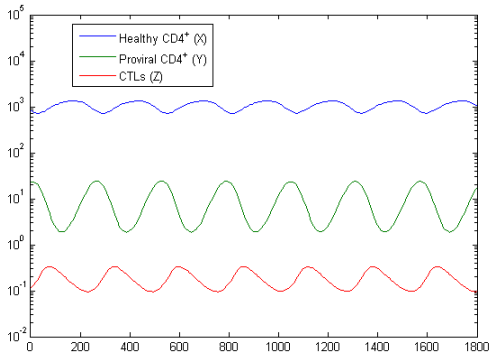

Figure 3.17: Numerical Solution to (M_1)-(M_3) with parameters as in (3.3.1)

In the case where $n = 2$ the given parameters result in super-critical Hopf bifurcations with respect λ, σ, γ, ν, a, μ_1, and μ_3. This is to be expected from what we have seen in the previous two sections, and therefore, we omit the

bifurcation diagrams for these parameters. Instead, we generate the bifurcation diagrams for β and μ_2 which both yield important results.

In the interest of comparing our results with that of Wodarz, Nowak, and Bangham (1999) [33] we demonstrate the existence of a super-critical Hopf bifurcation with respect to β.

Theorem 3.3.2 ***Super-critical Hopf Bifurcation with Respect to*** β
Consider the system (M) *with parameters given in Table 3.1. If* $n = 2$ *and* $\nu \cdot day \in (0.001, 0.081)$ *then this system undergoes a super-critical Hopf Bifurcation with respect to* β*.*

Proof: We consider the following bifurcation diagram produced in MATLAB using "bif2p.m". Since XPPAUT is unable to detect the stable periodic solutions we omit them. Nevertheless, the existence of a super-critical Hopf bifurcation with respect to β is clear from Figure 3.18.

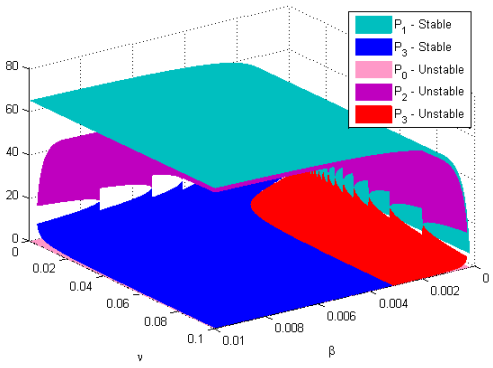

(a) Complete Bifurcation Diagram

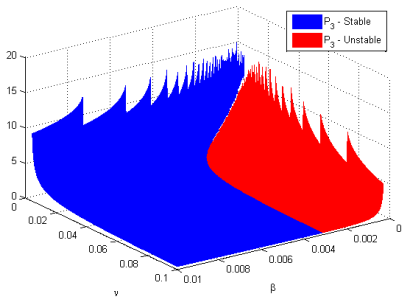

(b) Bifurcation Diagram Showing Only P_3

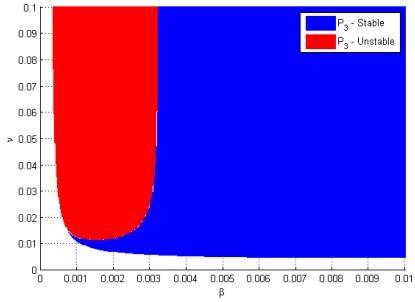

(c) Projection of P_3 into the β-ν Plane

Figure 3.18: Bifurcation with respect to β; parameters as in Table 3.1.

□

Finally, we note that when $n = 2$ we observe a sub-critical Hopf bifurcation with respect to μ_2.

Theorem 3.3.3 ***Sub-Critical Hopf Bifurcation with Realistic Parameters*** *Consider the system* (M) *with parameters given in Table 3.1. If* $n = 2$ *and* $\nu \cdot day \in (0.001, 0.081)$ *then this system undergoes a sub-critical Hopf Bifurcation with respect to* μ_2.

Proof: As usual, we proceed by using "bif2p.m" to generate the following bifurcation diagram. Unfortunately, we are unable to detect the unstable periodic solutions with XPPAUT or MATLAB. Nevertheless, the existence of the sub-critical Hopf bifurcation is clear from Figure 3.19.

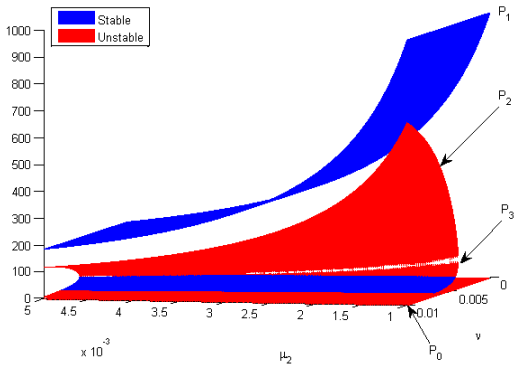

(a) Complete Bifurcation Diagram

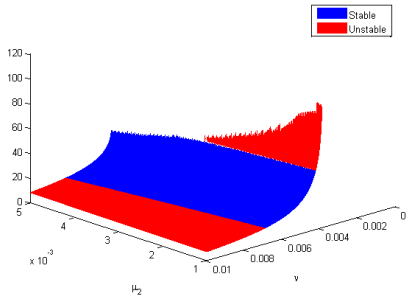

(b) Bifurcation Diagram Showing Only P_3

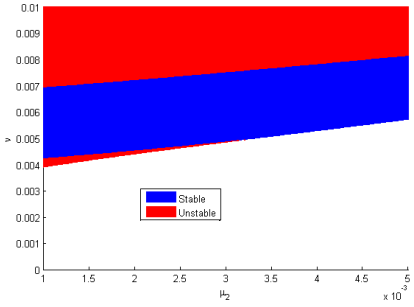

(c) Projection of P_3 into the μ_2-ν Plane

Figure 3.19: Bifurcation Diagrams with Respect to μ_2 and ν.

□

Chapter 4

Discussion

4.1 Summary

Before we proceed with our discussion it is beneficial to provide a summary of the previous two chapters. We start by discussing the various equilibria and their stability properties. Next, we revisit the Hopf bifurcations of P_3. Finally, we review our findings regarding simulations performed with realistic parameters.

The disease-free equilibrium, P_0, always exists. If $R_0 < 1$ then P_0 is globally asymptotically stable; otherwise it is unstable. Global asymptotic stability of P_0 precludes the existence of any other equilibria. Thus, in our discussion of the carrier and endemic equilibria we assume that $R_0 > 1$.

Consider next the carrier equilibrium, P_1. As mentioned above, the stability properties of P_0 imply that this equilibrium exists only if $R_0 > 1$. Together with Theorem 2.2.1 this gives that P_1 exists if and only if $R_0 > 1$. We prove that when P_1 exists it is locally asymptotically stable, see Theorem 2.3.1. Due to the existence of P_0 we are required to modify the definition of global asymptotic stability for P_1. Following this we identified sufficient conditions for P_1 to be globally asymptotically stable, see Theorem 2.3.2. In general, however, global asymptotic stability of P_1 is ruled out by the existence of P_2 and/or P_3.

The endemic equilibrium P_2 exists if $R_0 > 1$ and $\min_{\{z \in I\}} g(z) \leq 0$. Similarly, P_3 exists if $R_0 > 1$ and $\min_{\{z \in I\}} g(z) < 0$. Since $\min_{\{z \in I\}} g(z) = 0$ seems untenable for any real-world situation, our discussion of endemic equilibria assumes that $\min_{\{z \in I\}} g(z) < 0$. In particular, we do not deal with the case where P_2 exists and P_3 does not. Theorem 2.3.3 identifies a sufficient condition for the local asymptotic stability of P_2 and of P_3. Numerical simulations show that P_3 can be either stable or unstable, however, they fail to identify parameters for which P_2 is stable. This leads us to conjecture that P_2 is always unstable.

Under certain circumstances P_3 undergoes a Hopf bifurcation, see Theorems 2.3.5 and 3.1.1. Theorem 3.1.1 also indicates that these parameters result in a sub-critical Hopf bifurcation of P_3. Further investigation reveals that the system undergoes both sub- and super-critical Hopf bifurcations. Comparison with Gomez-Acevedo, Li, and Jacobson (*unpublished*) [9] indicates that the existence of Hopf bifurcations in our model results from the choice of CTL response function, $F(z) = \frac{yz^n}{z^n+a}$. Since both epidemiological and ecological models also make use of similar response functions, this result may have implications far beyond the modelling of HTLV-I.

The Hopf bifurcations of P_3 are robust in several respects. First, there are many different sets of parameters for which Hopf bifurcations occur. Second, we have observed that if one set of parameters gives rise to a Hopf bifurcation then it does so with respect to all parameters except n. Finally, the resulting stable or unstable periodic solutions persists for a relatively large range of the bifurcation parameter. In particular, Theorem 2.3.5 and 3.1.1 seem to indicate that the unstable periodic orbits observed in Figure 3.1 persist for all ν in some half-infinite interval.

The sub- and super-critical Hopf bifurcations result in unstable and stable periodic solutions, respectively. Although models for epidemiological, ecological, and immunological systems have been known to exhibit stable periodic solutions

[17, 24, 30, 33], unstable periodic solutions are rare. Indeed, this is the first immunological model for HTLV-I which allows for unstable periodic solutions. If the periodic orbit is unstable it is tempting to simply ignore it. However, doing so would neglect the interesting behaviour of solutions near the periodic solution.

The existence of solutions exhibiting prolonged transient oscillations allow us to "see" the unstable periodic solution. These prolonged transient oscillations lead us to conjecture that there is a stable manifold emanating from the periodic solution. The existence of a stable manifold is made more reasonable by the possibility that it may act as a partition between the basins of attraction of P_1 and P_3. Supporting evidence is provided numerically by showing that there are solutions converging to P_1 and to P_3 which exhibit transient oscillations and whose initial conditions are chosen to be close together, see Figures 3.6 and 3.7. In any case, the existence of these unstable periodic solutions constitutes an observable prediction not made by any previous HTLV-I model. Further discussions of some strategies for comparing immunological models for HTLV-I follow in Section 4.4.1.

Figures 3.6 and 3.7 also illustrate the bistability of our model. Theorems 2.2.1 and 2.3.1 state that the endemic equilibria can only exist if $R_0 > 1$ and that in this case P_1 is locally asymptotically stable, respectively. Thus, whenever P_3 or a periodic solution is locally asymptotically stable our system exhibits bistability. Bistability is not as rare a phenomenon in mathematical biology as are unstable periodic orbits; nonetheless, this is the first immunological model for HTLV-I which exhibits bistability between a carrier equilibrium and an endemic solution. Bistability plays a key role in the interpretation of this model and is indispensable in understanding phenomena left unexplained in previous models. Moreover, it provides another method for comparing our model against previous HTLV-I models.

Finally, an analysis of our model using realistic parameters estimated in Gomez-Acevedo, Li, and Jacobson (*unpublished*) [9] provides some interesting insights. For this realistic set of parameters we find both sub- and super-critical Hopf bifurcations. We show that there are super-critical Hopf bifurcations with respect to both λ and ν when $n = 2$ and when $n = 3$. We also show the presence of a sub-critical Hopf bifurcation with respect to μ_2. The presence of both super- and sub-critical Hopf bifurcations near the realistic set of parameters has interesting consequences to the biological interpretation of our model. This together with the resulting bistabililty constitutes the principal deviation of our model from previous ones and will form the focus of further discussion below.

4.2 Pathogenesis of HAM/TSP

In the Introduction, we stated two important questions being asked of HTLV-I infection.

1. Why is it that most people infected with HTLV-I remain asymptomatic carriers and only a few develop HAM/TSP?, and
2. Why is it that the disease develops after such a long incubation period?

We now attempt to address these questions beginning with a review of explanations proposed in previous works.

The specific works we will be considering are those of Gomez-Acevedo, Li, and Jacobson (*unpublished*) [9] and Wodarz, Nowak, and Bangham (1999) [33]. In both papers the final outcome is entirely determined by the choice of parameters. Thus, the explanation as to why only a small fraction of HTLV-I patients develop HAM/TSP would be that the fraction of the population with parameters corresponding to the existence of a globally asymptotically stable endemic solution[1] is small. Similarly, we would explain the long incubation period for

[1]When we use the term "endemic solution" we are referring to either an endemic equilibrium or a periodic orbit.

HTLV-I-associated HAM/TSP by proposing that as a person ages their immune system changes from a state where there is no endemic solution to one where there is a globally asymptotically stable endemic solution. Our model remains consistent with both of these interpretations, however, we discuss below some additional explanations for the above two questions which are unique to our model.

The bistability of our model provides an elegant answer to both of the above questions. We propose that so few people infected with HTLV-I develop HAM/TSP because, for the vast majority of people, exposure to HTLV-I places them in the basin of attraction of the carrier equilibrium, P_1. The long incubation period for HTLV-I-associated HAM/TSP can then be explained in two different ways.

Suppose that for some individual P_3 exists and is locally asymptotically stable. Also suppose that there exists an unstable periodic solution. The long incubation period in the development of HAM/TSP could then be explained as follows. An initial exposure to HTLV-I places the individual in the basin of attraction of P_3 and close to the stable manifold emanating from the unstable periodic solution. In this case they would experience prolonged transient oscillations in their CTL response. This transient behaviour could be responsible for the long incubation period of HAM/TSP. Indeed, the transient CTL behaviour may be insufficient to cause neurological damage. Alternatively, the neurological damage may occur in small bursts corresponding to spikes in the CTL response. In either case, they will ultimately approach the endemic equilibrium, P_3, where constant exposure to a strong CTL response corresponds to full-blown HAM/TSP.

Of course, the above scenario assumes only one exposure to HTLV-I. In reality, an individual may experience multiple exposures. Moreover, during the course of infection an individual will experience many other events which will perturb their orbit. These perturbations may be sufficient to move their solution from one basin

of attraction to the other. The relative likelihood of moving from one basin of attraction to another may further help to explain the rareness of HAM/TSP. These types of perturbations could also be invoked to explain the long incubation period of HAM/TSP. Indeed, suppose that for some individual a locally asymptotically stable endemic solution exists and that this individual's exposure to HTLV-I places them in the basin of attraction of the carrier equilibrium, P_1. They would then remain a carrier until such a time where they experience perturbations significant enough to move them into the basin of attraction of the endemic solution. The unlikelihood of such an event, or series of events, could explain the long incubation period observed before the development of HAM/TSP. If the endemic solution happens to be a periodic solution then it is possible that the disease may progress in small bursts corresponding to spikes in the CTL response, thus further contributing to the amount of time necessary for development of HAM/TSP.

The mechanisms of pathogenesis proposed above are, of course, purely speculative. In Section 4.4 we will explore some methods for clarifying the relative importance of the proposed explanations. First, however, we consider the implications of the above discussion to the treatment of HAM/TSP.

4.3 Treatment

Our above discussion gives rise to two different strategies for treatment of HTLV-I-associated HAM/TSP. First, one could alter the parameters of the model so that either P_0 or P_1 becomes globally asymptotically stable [2]. Second, one could perturb the orbit so that it enters the basin of attraction of P_1. In either case, the orbit will approach an equilibrium lacking a CTL response. Either strategy would thus result in at most a transient CTL response and there would be no need to worry about the long-term development of HAM/TSP.

[2]For our purposes, it is sufficient for P_1 to be asymptotically stable in $\text{int}(\Gamma)$ or even in $\text{int}(\Gamma) \setminus \{P_2, P_3\}$.

Models proposed by Gomez-Acevedo, Li, and Jacobson (*unpublished*) [9] and by Wodarz, Nowak, and Bangham (1999) [33], have lacked bistability; hence, their treatment options have been limited to fundamentally altering the parameters of the model. Our model is compatible with this interpretation and we briefly explore the specifics of this option.

Although we can identify scenarios resulting in the development of HAM/TSP it remains unclear which parameters give rise to these scenarios. Indeed, the precise effects of certain individual parameters is often difficult to ascertain. Part of this difficulty follows from our inability to determine a threshold parameter controlling the existence and/or stability of endemic solutions. Fortunately, however, the threshold parameter R_0 and Lemma 2.3.4 give useful insights into possible treatments for HTLV-I-associated HAM/TSP.

Recall that $R_0 = \frac{\lambda\sigma\beta}{\mu_1\mu_2}$ and that P_0 is globally asymptotically stable if and only if $R_0 \leq 1$. Theorem 2.3.1 gives that decreasing R_0 below 1 will result in clearing the HTLV-I infection. If instead of clearing the infection, however, all we are interested in is avoiding the development of HAM/TSP then decreasing R_0 below 1 may not be necessary. This is best illustrated by Figures 3.3(a), 3.3(b), 3.3(c), 3.4, and 3.5. In these figures, reproduced in Figure 4.1, decreasing R_0 results in P_2 and P_3 becoming unstable as well as the vanishing of any periodic solution. Since Γ is positively invariant, it is reasonable to expect that under these circumstances any solution in $\Gamma \setminus \{P_2, P_3\}$ will tend toward P_1, the carrier equilibrium. A similar behaviour is observed in Gomez-Acevedo, Li, and Jacobson (*unpublished*) [9].

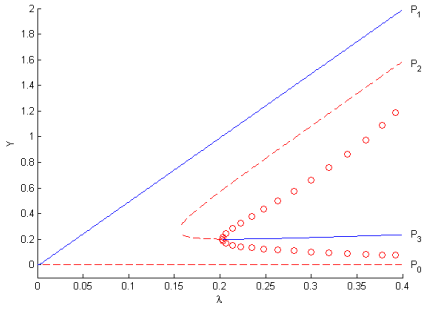

(a) 3.3(a), $R_0 = 1$ when $\lambda = 0.002$

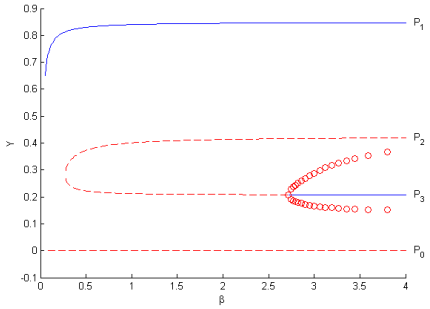

(b) 3.3(b), $R_0 = 1$ when $\beta \approx 0.0118$

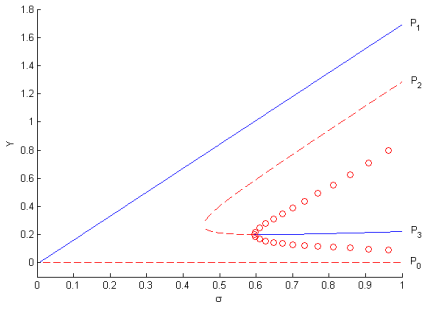

(c) 3.3(c), $R_0 = 1$ when $\sigma \approx 0.0059$

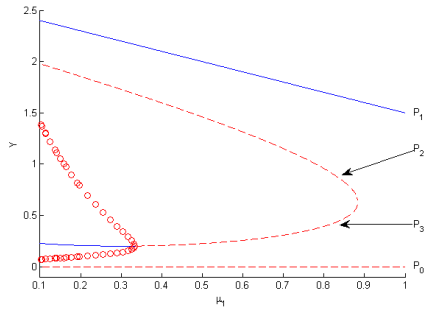

(d) 3.4, $R_0 = 1$ when $\mu_1 = 2.5$

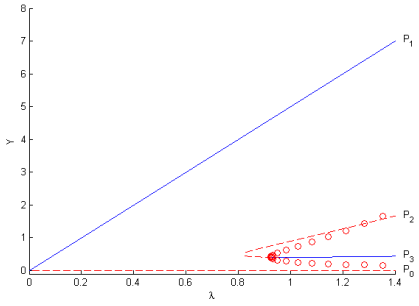

(e) 3.5, $R_0 = 1$ when $\lambda = 0.002$

Figure 4.1: Reproduction of Figures 3.3(a), 3.3(b), 3.3(c), 3.4, and 3.5.

When attempting to decrease R_0 we must keep in mind the biological context. For example, decreasing λ would decrease R_0. However, since λ represents the rate of production of new CD4$^+$ T-cells, a large decrease in λ may result in compromisation of the immune system. Increasing the rates of natural death of healthy CD4$^+$ T-cells, μ_1, would also lower R_0 with similar negative side effects. A more promising strategy might be to alter parameters which affect unhealthy CD4$^+$ T-cells. Specifically, we would wish to lower either β or σ, or to increase μ_2.

Altering these parameters would not necessarily affect the functioning of the immune system. Unfortunately, we can never be certain of avoiding side effects, as any treatment would require the use of pharmaceuticals with potentially unpleasant side effects.

For those parameters not in the expression for R_0 we can apply the methods of Lemma 2.3.4 to give us some insights into what a desirable treatment might be. For example, Figure 2.3 shows us that in order to treat HAM/TSP we should decrease the cytotoxic responsiveness, ν. As with decreasing λ or increasing μ_1, however, decreasing the cytotoxic responsiveness may result in compromisation of the immune system. Using a similar graph sketching strategy we see that it would be desirable to increase either μ_3, γ, or a. Of course, desirability is subject to the usual caveat of deleterious side effects.

While the models of Gomez-Acevedo, Li, and Jacobson (*unpublished*) as well as Wodarz, Nowak, and Bangham (1999) predict that treatment options are limited to altering parameters, we predict that it is possible to treat the disease by perturbing the orbit into the basin of attraction of P_1. Implementing this second strategy would seem to be much more delicate than implementing the first one. In particular, this strategy requires detailed knowledge of the shape size of the basins of attraction for P_1 and the locally asymptotically stable endemic solution. Information regarding the basin of attraction may be difficult to generate for several reasons. Computing the basins of attraction may be computationally intensive. Also, basins of attraction may be sensitive to perturbations in the parameters of the model. Thus, separate computations may be required for different individuals or even for the same individual during different stages of their life. Of course, the strategy of simply perturbing the orbit also has several significant advantages over altering the parameters of the system.

First we consider that fundamentally altering the parameters of the model would require a sustained effort and would be more costly than a mere perturbation of the system. Moreover, as we stressed above, such a sustained effort may result in side effects. We emphasize that side effects from sustained treatments can be severe. Indeed, the side effects of azidothimidine in the case study presented in Wodarz, Nowak, and Bangham (1999) [33] were so severe as to require a switch to a lamivudine treatment[3]. Finally, once the treatment is terminated the parameters of the system will revert to their default values. The consequences of this reversion depend on which model one uses for interpretation. We briefly explore the difference between our model and its predecessors below.

If we subscribe to either the Gomez-Acevedo, Li, and Jacobson (*unpublished*) [9] or Wodarz, Nowak, and Bangham (1999) [33] then a return to the default parameter values for someone in danger of developing HAM/TSP corresponds to the endemic equilibrium returning to globally asymptotically stable. So, unless the virus has been completely eliminated, termination of the treatment will eventually trigger a sustained CTL response and lead to HAM/TSP. Thus, these two previous models predict that successful treatment of HTLV-I-associated HAM/TSP must be ongoing. If, however, we subscribe to our model, then termination of this sort of treatment would not necessary result in a return to an endemic equilibrium. Ideally, treatment would be terminated when the orbit enters the basin of attraction of P_1 for default parameter values.

There are advantages and disadvantages to applying either of the two strategies discussed above. As far as side effects are concerned, it would appear as though simply perturbing the orbit may be a more successful strategy than fundamentally altering the parameters of the system. Since bistability of this nature is a novel feature of our model, however, this presupposes that our model is a more accurate representation of HTLV-I infection than its predecessors. This supplies us with an

[3]Both of these anti-retroviral treatments were intended to lower the infectiveness, β, of the HTLV-I virus.

excellent motivation to further explore the validity of all three of these models.

4.4 Future Work

We divide our discussion of future work into three categories. First, we consider methods for comparing our model against other HTLV-I models. Next, we discuss aspects of our model which have not been fully characterized and which require further analysis. Finally, we propose some different strategies for improving our current model.

4.4.1 Comparison of Models

The motivation behind pursuing further analysis of this and future models relies on the assumption of biological relevance. With at least two other reasonable models currently in circulation [9, 33] how can we tell which model deserves the most attention? Here we propose two different methods which could be used to determine which model provides the best fit. Both methods exploit differences in the predictions made by these models. In particular, we use that our model is the only one which predicts the existence of unstable periodic solutions and the existence of bistability.

We first consider how the existence of an unstable periodic solution may allow us to distinguish between models. Wodarz, Nowak, and Bangham (1999) [33] presents a series of data which illustrate rapid and prolonged oscillations in proviral load of a patient infected with HTLV-I undergoing anti-retroviral treatment. It is claimed that these oscillations are the product of a stable periodic solution resulting from a super-critical Hopf bifurcation induced by the anti-retroviral treatment. We suggest that the data presented does not follow the patient for long enough to make a conclusive determination on whether the oscillations observed are due to the presence of a stable periodic solution. Indeed, our model suggests an alternative explanation. As we have seen, Figure 3.7, our model allows for the

presence of prolonged oscillations due to the presence of an unstable periodic solution. In order to confirm the nature of these oscillations it would be wise to either re-analyze the data or repeat the experiment, keeping in mind the possibility of an unstable periodic solution.

Another strategy we could use to distinguish between models relies upon the bistability of our model. That the initial dose should have an effect on the progression of the disease is intuitively reasonable. Of course, it is not possible to proceed with experiments designed to verify this hypothesis. Fortunately, there may already exist a wealth of data which may yield evidence of bistability in the case of HTLV-I infection. From time to time an individual is transfused with HTLV-I contaminated blood. Such occurrences produce an opportunity to compare the prevalence of HAM/TSP in those infected with HTLV-I via blood transfusion to those infected by other means. These two different means of infection correspond to two significantly different sets of initial conditions.

Analyzing existing data in order to draw some conclusion on the likelihood of an individual developing HAM/TSP based on their method of infection poses considerable challenges. In particular, we must compensate for the fact that persons infected via blood transfusion are likely of poorer health than those infected by other means. Previous related studies give some hope of being able to accomplish this task. One study performed by Osame et. al. (1990) [27], for example, investigates similar aspects HTLV-I infection and HAM/TSP development via blood transfusion. Their determination of a higher prevalence of blood transfusion recipients among HTLV-I-associated HAM/TSP patients than among the general population is a promising result.

4.4.2 Further Analysis

Of all the equilibria of our model, only the behaviour of the disease free equilibrium, P_0, is fully understood. Specifically, if $R_0 \leq 1$ then P_0 is globally

asymptotically stable in Γ and it is unstable otherwise. The next best understood equilibrium is the carrier equilibrium, P_1, which only exists when $R_0 > 1$ and is always locally asymptotically stable. In Theorem 2.3.2 we identify sufficient conditions under which P_1 is globally asymptotically stable. We would also like to identify necessary conditions for the global asymptotic stability of P_1. In preparation for this, however, it is reasonable to investigate other sets of conditions which we suspect are sufficient for the global asymptotic stability of P_1.

We can name several situations under which we would expect P_1 to be locally asymptotically stable in some open subset of Γ. For example, for parameters where P_2 and P_3 do not exist ($\min_{z \in I} g(z) > 0$) we expect that P_1 would be globally asymptotically stable. Also, when P_2 and/or P_3 exist but are unstable we expect P_1 would be locally asymptotically stable inside $\text{int}(\Gamma) \setminus \{P_2, P_3\}$.

After coming to a more complete characterization of P_1, we would like to better understand the endemic equilibria, P_2 and P_3. In particular, it would be interesting to know whether or not we could find a single threshold parameter which determines the existence of these two equilibria. Since much of our analysis assumes that P_2 is always unstable, it would also be desirable to confirm this conjecture. As for P_3, we would like to know for what parameters it is stable or unstable, and also for what parameter values does it undergo a Hopf bifurcation.

Due to their importance, we would like to have a better understanding of the Hopf bifurcations present in this model. Ideally, it would be possible to identify necessary and sufficient conditions which give rise to a Hopf bifurcation. It would then be logical to analytically determine the nature of these Hopf bifurcations. For example, it would be interesting to prove that Hopf bifurcations resulting from Theorem 2.3.5 are sub-critical. It would be equally desirable to rigorously establish the existence of super-critical Hopf bifurcations. In addition, proving the existence of both of these types of Hopf bifurcation with respect to all parameters and for all

$n \geq 2$ would seriously strengthen the analysis of this model.

Bistability is another major phenomenon worthy of further investigation. In particular, our interpretation of this model with respect to HTLV-I infection would be greatly enhanced by knowing the relative size and shape of the basins of attraction of both P_1 and the endemic solutions. Furthermore, it would be interesting to see what magnitude of perturbation would be necessary to cause an orbit to move from one basin of attraction to another.

4.4.3 Improvements to Our Model

First, observe that as $n \to \infty$:

$$f(z) \overset{a.e.}{\to} \begin{cases} 0 & \text{if } 0 \leq z < 1 \\ 1 & \text{if } z \geq 1 \end{cases},$$

$$F(y,z) \overset{a.e.}{\to} \begin{cases} 0 & \text{if } 0 \leq z < 1 \\ y & \text{if } z \geq 1 \end{cases}.$$

Suppose then that we take this step response function instead of a sigmoidal response function. Applying the same argument as in Lemma 2.3.4 now results in there being at most one endemic equilibrium. In other words, P_2 no longer exists and P_3 is the only endemic equilibrium. This is not necessarily a major deviation from our current model due to the (seemingly) unstable nature of P_2. When using a step response function we would like to know whether the model retains all of the same behaviours as our current model. If so, then it may be desirable to work with such a step function. Indeed, there is no reason to believe that a step response function is any less reasonable than a sigmoidal response function. Moreover, a unique endemic equilibrium may simplify the calculations and the interpretation of the model.

In the introduction we made the simplifying assumption that there was no mitosis of healthy or proviral $CD4^+$ T-cells. This assumption greatly reduces the complexity of the model. However, there is substantial evidence to suggest that mitosis of healthy and proviral cells is extremely important to the dynamics of HTLV-I [3, 33]. Another simplifying assumption we made was that every proviral $CD4^+$ T-cell is constantly expressing the HTLV-I genome. In fact, there is evidence to suggest that the HTLV-I genome is dormant in most proviral cells [2, 3, 14]. This means that only a small fraction of proviral cells could either infect healthy $CD4^+$ T-cells or be detected by the CTL response. Reflecting on how critical these two assumptions are to the dynamics of HTLV-I highlights the importance of relaxing these assumptions.

Bibliography

[1] B. Asquith and C.R.M. Bangham. *Quantifying HTLV-I dynamics. Immunology and Cell Biology*, 85:280–286, 2007.

[2] B. Asquith, A.J. Mosley, A. Heaps, and four more authors. *Quantification of the virus-host interaction in human T lymphotropic virus I infection. Retrovirol.*, 2:75–83, 2005.

[3] B. Asquith, Y. Zhang, A.J. Mosley, and twelve more authors. *In vivo T lymphocyte dynamics in humans and the impact on human T-lymphotropic virus 1 infection. PNAS*, 104:8035–8040, 2007.

[4] C.R. Bangham. *The immune control and cell-to-cell spread of human T-lymphotropic virus type 1. J. of Gen. Virol.*, 84:3177–3189, 2003.

[5] M. Cavrois, S. Wain-Hobson, A. Gessain, and two more authors. *Adult T-Cell Leukemia/Lymphoma on a Background of Clonally Expanding Human T-Cell Leukemia Virus Type-1-Positive Cells. Blood*, 88:4646–4650, 1996.

[6] J.M. Coffin, S.H. Hughes, and H.E. Varmus. *Retroviruses.* Cold Spring Harbor Laboratory Press, Cold Spring Harbor, NY, 1997.

[7] G. de The and R. Bomford. *An HTLV-I vaccine: why, how, and for whom? AIDS Res. Hum. Retroviruses*, 9:381–386, 1993.

[8] R.C. Gallo. *History of the discoveries of the first human retroviruses: HTLV-1 and HTLV-2. Oncogene*, 24:5926–5930, 2005.

[9] H. Gomez-Acevedo, M. Li, and S. Jacobson. *Multi-Stability in a Model for CTL Response to HTLV-I Infection and its Consequences in HAM/TSP Development and Prevention.*

[10] H. Gomez-Acevedo and M.Y. Li. *Global Dynamics of a Mathematical Model for HTLV-I Infection of T Cells. Canadian Appl. Math. Quart.*, 10:71–86, 2002.

[11] H. Gomez-Acevedo and M.Y. Li. *Backward bifurcation in a model for HTLV-I infection of CD4$^+$ T cells. Bull. Math. Biol.*, 67:101–114, 2005.

[12] M.M. Gore, J.P. Thakare, S.N. Ghosh, and R.S. Wadia. *Are these autoimmune disorder induced by altered antigens? Arch. Neurol.*, 45:601–602, 1988.

[13] O. Gout, M. Baulac, A. Gessain, and seven more authors. *Medical Intelligence: Rapid Development of Myelopathy after HTVL-I Infections Acquired by Transfusion During Cardiac Transplantation. N. Engl. J. Med.*, 322:383–388, 1990.

[14] P. Hollsberg and D.A. Hafler. *Pathogenesis of Diseases Induced by Human Lymphotropic Virus Type I Infection. N. Engl. J. Med.*, 328:1173–1182, 1993.

[15] S. Ijichi, S. Izumo, N. Eiraku, and eight more authors. *An autoaggressive process against bystander tissues in HTLV-I-infected individuals: a possible pathomechanism of HAM/TSP. Med. Hypotheses*, 42:542–547, 1993.

[16] Y. Ina and T. Gojobori. *Molecular Evolution of Human T-Cell Leukemia Virus. J. Mol. Evol.*, 31:493–499, 1990.

[17] S. Iwami, Y. Takeuchi, Y. Miura, and two more authors. *Dynamical properties of autoimmune disease models: Tolerace, flare-up, dormancy. J. Theo. Biol.*, 246:646–659, 2007.

[18] Y. Iwasaki, Y. Ohara, I Kobayashi, and S.I. Akizuki. *Infiltration of Helper/Inducer T Lymphocytes Heralds Central Nervous System Damage in Human T-cell Leukemia Virus Infection. Am. J. Path.*, 140:1003–1008, 1992.

[19] S. Jacobson. *Immunopathogenesis of Human T Cell Lymphotropic Virus Type I-Associated Neurologic Disease. J. of Infect. Dis.*, 186:S187–S192, 2002.

[20] Y. Koyanagi, Y. Itoyama, N. Nakamura, and five more authors. *In vivo infection of human T-cell leukemia virus type I in non-T cells. Virology*, 196:25–33, 1993.

[21] R. Kubota, M. Osame, and S. Jacobson. *Effects of Microbes on the Immune System*, chapter Retrovirus: HTLV-I-Associated Diseases, pages 349–371. Lippincott Williams & Wilkins, 2000.

[22] T.J. Lehky, C.H. Fox, S. Koenig, and seven more authors. *Detection of Human T-Lymphotropic Virus Type I (HTLV-I) Tax RNA in the Central Nervous System of HTLV-I-associated Myelopathy/Tropical Spastic Paraparesis Patients by In Situ Hybridization. Ann. Neurol.*, 37:167–175, 1995.

[23] O. Lejeune, M.A.J. Chaplain, and I. El Akili. *Oscillations and bistability in the dynamics of cytotoxic reactions mediated by the response of immune cells to solid tumours. Math. Comput. Modelling*, 47:649–662, 2008.

[24] W. Liu, H.W. Hethcote, and S.A. Levin. *Dynamical behaviour of epidemiological models with nonlinear incidence rates. J. Math. Biol.*, 25:359–380, 1987.

[25] E. Matsuoka, N. Takenouchi, K. Hashimoto, and seven more authors. *Perivascular T cells are infected with HTLV-I in the spinal cord lesions with HTLV-I-associated myelopathy/tropical spastic paraparesis: double staining of immunohistochemistry and polymerase chain reaction in situ hybridization. Acta Neuropathol.*, 96:340–346, 1998.

[26] M.A. Nowak and R.M. May. *Virus Dynamics: Mathematical Principles of Immunology and Virology.* Oxford University Press, Great Clarendon Street, Oxford, 2000.

[27] M. Osame, R. Janssen, H Kubota, and eight more authors. *Nationwide Survey of HTLV-I-associated Myelopathy in Japan: Association with Blood Transfusion. Ann. Neurol.*, 28:50–56, 1990.

[28] L. Real. *The kinetics of functional response. American Naturalist*, 111:289–300, 1977.

[29] J. Stark, C. Chan, and A.J.T. George. *Oscillations in the immune system. Immunol. Rev.*, 216:213–231, 2007.

[30] J. Swart. *A system dynamics approach to predator-prey modeling. System Dyn. Rev.*, 6:94–99, 1990.

[31] L. Wang, M.Y. Li, and D. Kirschner. *Mathematical analysis of the global dynamics of a model for HTLV-I infection and ATL progression. Math. Biosci.*, 179:207–217, 2002.

[32] D. Wodarz and C.R.M Bangham. *Evolutionary Dynamics of HTLV-I. J. Mol. Evol.*, 50:448–455, 2000.

[33] D. Wodarz, M.A. Nowak, and C.R.M Bangham. *The dynamics of HTLV-I and the CTL response. Immunol. Today*, 20:220–227, 1999.

Appendix A

M-Files and ODE Files

A.1 M-Files

For all M-files below, we consider p to be a vector of length 10 which contains parameter values in the following order:

$$p = [\lambda, \beta, \sigma, \gamma, \nu, a, \mu_1, \mu_2, \mu_3, n].$$

For ease of viewing all comments are colored green and all non-standard functions (i.e. functions for which an M-file is included in this section) are colored red.

```
%  Accepts parameters "p".  "select" chooses
% param. to be varied, "range" is the range over
% which the param. will be varied, and "mesh" is
% the step size.

function bif(p,select,range, mesh)

k = floor((range(2)-range(1))/mesh);

%  Column 1: param values p(select).  Columns 3,
% 5, and 7: y component for equil P1, P2, & P3.
% Columns 2, 4, 6, and 8: 1 if the equil. in P0,
% P1, P2, or P3 is stable, -1 if it is unstable,
% 0 if it does not exist.

data = zeros(k,8);

%  Row 1: No. of stable equil.  Row 2: No. of
% unstable equil.  Col 1-4 are for P0-P3.

n = zeros(2,4);

for i = 1:k
    p(select) = range(1)+mesh*(i-1);
    data(i,1) = p(select);
    R0 = p(1)*p(2)*p(3)/(p(7)*p(8));
    if R0 <= 1
        n(1,1) = n(1,1)+1;
        data(i,2) = 1;
    else
        n(2,1) = n(2,1)+1;
        data(i,2) = -1;
        n(1,2) = n(1,2)+1;
        data(i,3) = p(7)*(R0-1)/p(2);
        data(i,4) = 1;
    end
    [z1,z2,data(i,6),data(i,8)] = p2p3(p);
    if z1 > 0
        data(i,5) = (p(1)*p(2)*p(3)-p(7)*p(8)-
p(7)*p(4)*z1)/(p(2)*p(8)+p(2)*p(4)*z1);
    end
    if z2>0
        data(i,7)=(p(1)*p(2)*p(3)-p(7)*p(8)-
p(7)*p(4)*z2)/(p(2)*p(8)+p(2)*p(4)*z2);
    end

    for l=3:4
        if data(i,2*l)==1
            n(1,l)=n(1,l)+1;
        elseif data(i,2*l)==-1
            n(2,l)=n(2,l)+1;
        end
    end

end

hold on

for i = 1:2
    for j = 1:4
        if n(i,j) > 0
            x = data(:,1);
            y = zeros(k,1);
            for l = 1:k
                if j==1 && data(l,2)==(-1)^(i-1)
                    y(l) = 0;
                elseif j>1 && data(l,2*j)==(-
1)^(i-1) && data(l,2*j-1)>0
                    y(l) = data(l,2*j-1);
                else
                    y(l) = NaN;
                end
            end
            if i==1
                plot(x,y,'-b')
            else
                plot(x,y,'--r')
            end
        end
    end
end
```

Figure A.1: bif.m

```
%  Accepts parameters p.  "select": param to be
% varied; "range": range over which the params will
% be varied; and "mesh": step size.
function n = bif2p(p,select,range, mesh)
k = zeros(1,2); %  "k": no. of pts select(1)/(2).
for i=1:2
    k(i)=floor((range(i,2)-range(i,1))/mesh(i))+1;
end
%  "data" stores all data collected.  The first two
% columns: param. values for select(1)/(2).  Columns
% 4, 6, and 8: y component for equil P1, P2, and P3.
% Columns 3, 5, 7, and 9: 1 if the equil. in P0, P1,
% P2, or P3 is stable, -1 if it unstable, 0 if DNE.
data=zeros(k(1)*k(2),9);
%  "n" Row 1: no. of stable equil.  Row 2: no. of
% unstable equil.  Col 1-4 are for P0-P3.
n=zeros(2,4);
for i=1:k(1)
    for j=1:k(2)
        row =  (i-1)*k(2)+j;
        data(row,1)=range(1,1)+mesh(1)*(i-1);
        data(row,2)=range(2,1)+mesh(2)*(j-1);
        p(select(1))=data(row,1);
        p(select(2))=data(row,2);
        R0 = p(1)*p(2)*p(3)/(p(7)*p(8));
        if R0<=1
            n(1,1)=n(1,1)+1;
            data(row,3)=1;
        else
            n(2,1)=n(2,1)+1;
            data(row,3)=-1;
            n(1,2)=n(1,2)+1;
            data(row,4)=p(7)*(R0-1)/p(2);
            data(row,5)=1;
        end
        [z1,z2,data(row,7),data(row,9)]=p2p3(p);
        if z1>0
            data(row,6)=(p(1)*p(2)*p(3)
            -p(7)*p(8)-p(7)*p(4)*z1)
            /(p(2)*p(8)+p(2)*p(4)*z1);
        end
        if z2>0
            data(row,8)=(p(1)*p(2)*p(3)
            -p(7)*p(8)-p(7)*p(4)*z2)
            /(p(2)*p(8)+p(2)*p(4)*z2);
        end
        for l=3:4
            if data(row,2*l+1)==1
                n(1,l)=n(1,l)+1;
            elseif data(row,2*l+1)==-1
                n(2,l)=n(2,l)+1;
            end
        end
    end
end
%  Plot surfaces.
x=zeros(1,k(1));
y=zeros(1,k(2));
for i=1:k(1)
    x(i)=range(1,1)+(i-1)*mesh(1);
end
for i=1:k(2)
    y(i)=range(2,1)+(i-1)*mesh(2);
end
for i=1:2
    for j=1:4
        z=zeros(k(2),k(1));
        for l=1:k(1)
            for m=1:k(2)
                pos=(l-1)*k(2)+m;
                if data(pos,2*j+1)==(-1)^(i-1)
                    if j>1
                        z(m,l)=data(pos,2*j);
                    end
                else
                    z(m,l)=NaN;
                end
            end
        end
        if i==1 && n(i,j)>0
    surf(x,y,z,'FaceColor','Blue','EdgeColor','Blue')
        elseif i==2 && n(i,j)>0
    surf(x,y,z,'FaceColor','Red','EdgeColor','Red')
        end
        hold on
    end
end
```

Figure A.2: bif.m

```
%  Verifies the four conditions in Hopf
% Bifurcation Theorem

function HBVerification(p)

% HB1
if p(9)*p(10)/p(7) <= 1
    HB1 = 'true'
else
    HB1 = 'false'
end

% HB2
R0 = p(1)*p(2)*p(3)/(p(7)*p(8));
c = [1,0,0];
c(2) = -p(8)/p(4)*( (p(10)-1)*R0/p(10)-2 );
c(3) = -(p(8)/p(4))^2*(R0-1);
psi = max(roots(c));

if psi < p(8)/p(4)*(R0-1)
    HB2 = 'true'
else
    HB2 = 'false'
end

% HB3
if p(6)*(p(10)-1) < (p(8)/p(4)*(R0-1))^p(10)
    HB3 = 'true'
else
    HB3 = 'false'
end
```

```
% HB4
% If xi < z^*(nubar) then nubar = nuhat.
% Otherwise, we calculate nuhat.
[zstar,nubar] = zstarnubar(p,0.001);

if xi < zstar
    zhat = zstar;
    p(5) = nubar;
else
    p(5) = zinv(p,xi,0.001);
    [z1,z2] = p2p3(p);
    zhat = max([z1,z2]);
end

% Calculate m = (Mtr-det)_P2(\hat{\nu})
c1 = p(1)*p(2)*p(3)/(p(8)+p(4)*zhat);
c2 = (p(1)*p(2)*p(3)-p(7)*p(8)-
p(7)*p(4)*zhat);
c3 = p(9)*(p(6)*(p(10)-1)-
zhat^p(10))/(p(6)+zhat^p(10));

m = -c1*c2 + c1^2*c3 - c1*c3^2 +
c3*p(4)*p(9)*zhat;

if m >0
    HB4 = 'true'
else
    HB4 = 'false'
end
```

Figure A.3: HBVerification.m

```
%  If g(z) has positive roots it returns them
% as z1<z2.  If zi is stable then si=1, if zi
% is unstable then si=-1, otherwise si=0.  If
% g(z) has no positive roots % then zi=0.

function [z1,z2,s1,s2] = p2p3(p)

c = zeros(p(10)+2,1);

if p(10) > 2
c(p(10)+2) = p(2)*p(6)*p(8)*p(9);
c(p(10)+1) = p(2)*p(4)*p(6)*p(9);
     c(3) = p(5)*p(7)*p(8)
     - p(1)*p(2)*p(3)*p(5);
     c(2) = p(2)*p(8)*p(9) + p(4)*p(5)*p(7);
     c(1) = p(2)*p(4)*p(9);
else
c(4) = p(2)*p(6)*p(8)*p(9);
c(3) = p(2)*p(4)*p(6)*p(9) + p(5)*p(7)*p(8)
     - p(1)*p(2)*p(3)*p(5);
c(2) = p(2)*p(8)*p(9) + p(4)*p(5)*p(7);
c(1) = p(2)*p(4)*p(9);
end

r = roots(c);
```

```
% For counting the number of roots use 'n'.
n = 0;
z = zeros(2,1);

for i = 1:p(10)+1
    if real(r(i))==r(i) && r(i)>0 && n==0
        z(1) = r(i);
        n=n+1;
    elseif real(r(i))==r(i) && r(i)>0 && n==1
        z(2) = r(i);
        n=n+1;
    end
end

z1 = min(z);
z2 = max(z);

if z1>0
    s1 = stability(p,z1);
else
    s1=0;
end

if z2>0
    s2 = stability(p,z2);
else
    s2=0;
end
```

Figure A.4: p2p3.m

```
%  x0 is the centre of a circle (rad. r) of points
% (separated by 2pi/num radians) in the plane normal to
% f(x0) (x'=f(x)).  Run simulations with these IC.
% Assume only P1 and P2 are stable.  If the solution
% has not converged to P1 after k iterations then
% assume convergence to P2. tol determines the
% tolerance for conv. to P1.
%
%  NOTE: If convergent to P1 then points(4,i)=1, else
% points(4,i)=2.
%  NOTE: T gives us two points one of which goes to P1
% the other of which goes to P2. These two points are
% as close as possible.

function [xP1,xP2,T]=psolnsM(p,r,num,x0,tol,k)
n = [p(1)-p(2)*x0(1)*x0(2)-p(7)*x0(1),
     p(2)*p(3)*x0(1)*x0(2)-p(4)*x0(2)*x0(3)-p(8)*x0(2),
     p(5)*(x0(2)*x0(3)^2)/(p(6)+x0(3)^2)-p(9)*x0(3)];
a = [0,-x0(2),x0(2)*n(2)/n(3)];
a = a/norm(a);
b = cross(a,n);
b = b/norm(b);
T = [[a(1),b(1),n(1)];[a(2),b(2),n(2)];
[a(3),b(3),n(3)]];
IC = zeros(3,num); %Initial conditions for simulation
for i=1:num
    theta = 2*pi*i/num;
    IC(1,i) = r*cos(theta);
    IC(2,i) = r*sin(theta);
end
IC = T*IC;
for i=1:num
    IC(:,i)=IC(:,i)+x0;
end
P1 = [p(8)/(p(2)*p(3)),
     p(7)*(p(1)*p(2)*p(3)/(p(7)*p(8))-1)/p(2),0];
[z1,z2,s1,s2]=p2p3(p);
if s1==1
   P2=[(p(8)+p(4)*z1)/(p(2)*p(3)),
       (p(1)*p(2)*p(3)-p(7)*p(8)-
     p(7)*p(4)*z1)/(p(2)*p(8)+p(2)*p(4)*z1),z1];
elseif s2==1
    P2=[(p(8)+p(4)*z2)/(p(2)*p(3)),
   (p(1)*p(2)*p(3)-p(7)*p(8)-
     p(7)*p(4)*z2)/(p(2)*p(8)+p(2)*p(4)*z2),z2];
end
% Make sure that tol is small enough.
if 2*tol >= norm(P1-P2)
    tol = norm(P1-P2)/3;
end
% Begin simulation.
points = zeros(4,num);
nP1 =0; % Number of solutions converging to P1.
for i=1:num
    x=[IC(1,i);IC(2,i);IC(3,i)];
    points(:,i) = [IC(1,i);IC(2,i);IC(3,i);0];
    [time,Y] = ode45(@odefun,[0,k],x);
    [a,b]=size(Y);
    x = [Y(a,1),Y(a,2),Y(a,3)];
    if norm(x-P2)<=tol
        points(4,i)=2;
    elseif norm(x-P1)<=tol
        points(4,i)=1;
        nP1=nP1+1;
    end
end
xP1 = zeros(3,nP1); % xP? are IC which converge to P?
xP2 = zeros(3,num-nP1);
T = zeros(3,2);
tempy =1;
for i=1:num
    if points(4,i)==1
     xP1(:,tempy)=[points(1,i);points(2,i);
             points(3,i)];
        tempy=tempy+1;
    elseif points(4,i)==2
        xP2(:,i+1-tempy)=[points(1,i);points(2,i);
           points(3,i)];
    end
    if i>1 & points(4,i)+points(4,i-1)==3
        T = [[points(1,i-1),points(1,i)];
             [points(2,i-1),points(2,i)];
             [points(3,i-1),points(3,i)]];
    end
end
scatter3(xP1(1,:),xP1(2,:),xP1(3,:),'MarkerEdgeColor',
'Blue','MarkerFaceColor','Blue')
hold on
scatter3(xP2(1,:),xP2(2,:),xP2(3,:),'MarkerEdgeColor',
'Red','MarkerFaceColor','Red')
```

Figure A.5: pSolns.m

```
%  Accepts parameter array p and equilibrium
z.
% Returns 1 if z is stable, -1 if unstable, 0
% if unknown.

function s = stability(p,z)

x = (p(8)+p(4)*z)/(p(2)*p(3));
y = (p(1)-p(7)*x)/(p(2)*x);

A = [
[-p(2)*y-p(7), -p(2)*x, 0];
[p(2)*p(3)*y, p(2)*p(3)*x-p(4)*z-p(8),
     -p(4)*y];
          [0, p(5)*z^p(10)/(z^p(10)+p(6)),
          p(10)*p(5)*p(6)*y*z^(p(10)-
          1)/((z^p(10)+p(6))^2)-p(9)]
    ];

d = eig(A);

if real(d(1))<0 && real(d(2))<0 &&
real(d(3))<0
    s = 1;
elseif
real(d(1))>0||real(d(2))>0||real(d(3))>0
    s = -1;
else
    s = 0;
end
```

Figure A.6: stability.m

```
%  Calculates the \nu which gives z0 as the
% largest positive root of g(z) to a specified
% tolerance, tol.

function nu = zinv(p,z0,tol)

% Initialize p(5) to nubar
[z,p(5)] = zstarnubar(p,tol);

a = p(5);

while z-z0 <= 0
    p(5) = p(5)*2;

    [z1,z2] = p2p3(p);

    z = max([z1,z2]);
end

b = p(5);

while b-a > tol
    p(5) = (b+a)/2;

    [z1,z2] = p2p3(p);

    z = max([z1,z2]);

    if z-z0 > 0
        b=p(5);
    else
        a=p(5);
    end
end

nu=p(5);
```

Figure A.7: zinv.m

```
%  Calculates zstar evaluated at nubar within
% a tolerance of tol using the method of
% bisection.  Outputs [zstar,nubar].

function [zstar,b] = zstarnubar(p,tol)

% Initialize p(5) to a non-zero number

p(5) = 1;

[z1,z2] = p2p3(p);

if z1 > 0 && z2 > 0
    a = 0;
    b = p(5);
else
    a = p(5);
    while z1 <= 0 || z2 <= 0
        p(5) = p(5)*2;
        [z1,z2] = p2p3(p);
    end
    b = p(5);
end

while abs(z1-z2) > tol
    p(5) = (a+b)/2;
    [z1,z2] = p2p3(p);

    if z1 > 0 && z2 > 0
        b = p(5);
    else
        a = p(5);
    end

    p(5) = b;
    [z1,z2] = p2p3(p);
end

p(5) = b;
[z1,z2] = p2p3(p);
zstar = min([z1,z2]);
```

Figure A.8: zstarnubar.m

A.2 ODE Files

```
# Model
dx/dt=lambda-mu1*x-beta*x*y
dy/dt=sigma*beta*x*y-mu2*y-gamma*y*z
dz/dt=nu*(y*z^n)/(a+z^n)-mu3*z

# Initial Condition
x(0)=2.1428
y(0)=0.2974
z(0)=0.5743

# Parameters
param lambda=2.78,beta=1,sigma=1
param gamma=1.99,nu=3.26,a=0.45
param mu1=1,mu2=1,mu3=0.5,n=3

done
```

Figure A.9: model.ode